A low CDKN1c/p57^{kip2} expression in spinal progenitors drives the transition from proliferative to neurogenic modes of division

Baptiste Mida [1], Nathalie Lehman [2], Fanny Coulpier [3], Kamal Bouhali [1], Rosette Goiame [1], Morgane Thomas-Chollier [2,4], Evelyne Fischer [5*], Xavier Morin [6*]

1 : Institut de Biologie de l'Ecole Normale Supérieure (IBENS), CNRS, Inserm, Ecole Normale Supérieure, Sorbonne University, Collège Doctoral, 75005 Paris, France.

2 : Institut de Biologie de l'ENS (IBENS), Département de biologie, École normale supérieure, CNRS, INSERM, Université PSL, 75005 Paris, France

3 : Genomique ENS, Institut de Biologie de l'ENS (IBENS), Département de biologie, École normale supérieure, CNRS, INSERM, Université PSL, 75005 Paris, France

4 : Institut universitaire de France (IUF)

5 : Institut de Biologie de l'Ecole Normale Supérieure (IBENS), CNRS, Inserm, Ecole Normale Supérieure, PSL Research University, 75005 Paris, France. Electronic address: evelyne.fischer@ens.fr

6 : Institut de Biologie de l'Ecole Normale Supérieure (IBENS), CNRS, Inserm, Ecole Normale Supérieure, PSL Research University, 75005 Paris, France. Electronic address: xavier.morin@ens.fr

* : co-last authors ; co-corresponding authors

Keywords: neurogenesis, cell cycle, neurogenic switch, Cdkn1c, single cell transcriptomics

ABSTRACT

During vertebrate neurogenesis, a progressive transition from symmetric proliferative to asymmetric neurogenic progenitor divisions is critical to balance growth and differentiation. We used single-cell RNA-seq data from chick embryonic neural tube to characterize the molecular mechanisms that drive this transition. Here we show that Cdkn1c, a key cell cycle regulator which is classically associated with neuronal cell cycle exit, plays an earlier role during neurogenesis by favoring a shift towards neurogenic mode of division. Cdkn1c expression progressively increases in neural progenitors, and its knock down leads to a reduction of neuron production, following a shortening of cell cycle mainly attributed to a reduction in G1 duration. Clonal analysis of pairs of sister cells indicates that reducing Cdkn1c expression in progenitors delays neurogenesis by favoring a symmetric proliferative mode of division. Combined CyclinD1 and Cdkn1c knockdowns restores the cell cycle defects and a wild-type distribution of modes of division, indicating that Cdkn1c acts via the regulation of cell cycle parameters. We propose a sequential role for Cdkn1c in neuron production, with its progressive expression in progenitors first promoting neurogenic division patterns via cell-cycle lengthening, before mediating cell cycle exit in daughter cells.

INTRODUCTION

The vertebrate central nervous system (CNS) is a complex assembly of thousands of cell types, which are organized in an exquisite manner to form functional neural circuits. This amazing diversity develops through the sequential production of neuronal and glial cells from a limited pool of neuroepithelial stem cells (also called neural progenitors) (Noctor et al., 2001; Taverna et al., 2014). Precise coordination between growth and differentiation during the neurogenic period is paramount to produce the correct amount of brain cells "at the right place at the right time" and ensure the formation of neural circuits. To achieve this complex organization, both the number of times progenitors enter a cell cycle, and the proportion of progenitors that exit cell cycle at each round of division are crucial. A tight regulation of the proliferative capacity of the progenitor itself (the number of times it divides) coordinated with neuronal fate determination in daughter cells is required to simultaneously produce early neurons, and maintain a pool of cycling progenitors that will generate later born neurons and eventually glial cells.

After a phase of amplification via proliferative symmetrical divisions, during which a precursor produces two progenitors, the progenitor pool progressively switches to a "neurogenic" phase to initiate neuron production. During this phase, progenitors first perform asymmetric divisions that allow the simultaneous maintenance of a progenitor and production of a committed progeny, and later switch to terminal symmetric divisions producing two committed daughter cells (Taverna et al., 2014). Clonal analyses in the mouse and rat embryonic cortex indicate that progenitors that have undergone a neurogenic division do not normally reenter a proliferative state, suggesting an irreversible switch in competence (Gao et al., 2014; Noctor et al., 2004, 2001). Several studies have identified differences in transcriptomic and chromatin landscapes between proliferative and neurogenic progenitors (Aprea et al., 2013; Arai et al., 2011; Haubensak et al., 2004a; Iacopetti et al., 1999; Murielle Saade et al., 2013; (Albert et al., 2017) As an example, expression of the Tis21/BTG2/PC3 transcription factor is initiated during the switch from proliferation to neurogenesis from the forebrain (Iacopetti et al., 1999) to the spinal cord, in both the mouse (Haubensak et al., 2004b) and chick model (Hämmerle et al., 2002; Murielle Saade et al., 2013). These observations suggest that the two types of progenitors correspond to two distinct and successive stages in the neural developmental program.

Here, we sought to identify drivers of the neurogenic transition in the developing spinal cord. The lower cellular complexity of the spinal cord compared to the cortex, and its reliance on direct neurogenesis, represent an advantage to address this question. We used single-cell RNA sequencing (scRNAseq) data from embryonic chick spinal neural tube to explore the changes in gene expression that underlie the progression from proliferative to neurogenic progenitor states, and identified several genes differentially expressed during the neurogenic transition. One of the most striking candidates was the CDK inhibitor CDKN1c/p57Kip2 (thereafter referred to as CDKN1c) (Matsuoka et al., 1995) ; (Lee et al., 1995), a cell cycle regulator known to drive cell cycle exit in newborn neurons of the vertebrate CNS (Gui et al., 2007; Mairet-Coello et al., 2012a; Tury et al., 2011). Strikingly, our analysis established that it is already expressed in a subset of cycling spinal cord progenitors. We therefore postulated that Cdkn1c may also be acting earlier in the process of neuron production, as an actor in the switch towards neurogenic modes of division, and we went on to functionally explore this additional role in the chick embryonic spinal cord.

Using a knock-down strategy, we demonstrated that delaying Cdkn1c expression in cycling progenitors impedes the lengthening of the cell cycle that is normally observed at the start of neurogenesis, and reduces neuron production. Clonal analysis of the fate of the daughter cells born from CDKN1c-depleted progenitors showed an increase in progenitor fate, involving the onset of Cdkn1c expression in progenitors in the switch from proliferative to neurogenic modes of division. Conversely, we showed that advancing CDKN1c expression onset via low-level overexpression in proliferative progenitors is sufficient to convert them to a neurogenic mode of division. Combining CyclinD1 and CDKN1c knockdowns restores both cell cycle parameters and a wild-type distribution of modes of division, indicating that Cdkn1c acts mainly via inhibition of the CyclinD1/CDK6 complex. Taken together, our results show that a progressive increase in Cdkn1c expression regulates two successive steps in the production of spinal cord neurons: intermediate levels in progenitors induce a switch from a proliferative to a neurogenic mode of division, while a higher expression in newborn neurons favors cell cycle exit and differentiation.

RESULTS

1) Transcriptional signature of the neurogenic transition.

We used single-cell transcriptomics (scRNAseq) to identify critical differences in gene expression between proliferative and neurogenic populations which could drive the progressive transition from the proliferative to the neurogenic state.

We therefore chose to analyse scRNAseq data from embryonic spinal neural tubes, which rely only on direct neurogenesis and in which progenitors are more homogeneous compared to cortical progenitors (Taverna et al., 2014). We produced scRNAseq data from the cervical neural tube region of chick embryos at HH18 (E2.75), a stage at which proliferative and neurogenic modes of division are about equally represented (Bonnet et al., 2018; M. Saade et al., 2013). To overcome limitations in the number of reads assigned to genes resulting from the poor annotation of many genes' 3'UTRs in the chick genome, we developed a reannotation strategy based on bulk long-read RNA-seq from matched tissue (see Methods). This considerably improved the assignment of scRNAseq reads to genes and therefore the count of expressed genes in each cell.

We restricted our analyses from the original dataset to central nervous system-related cells (1878 cells) (Figure 1A), excluding neural crest and mesoderm derivatives (see Methods). In UMAP representations (Figure 1B), these cells do not seem to arrange in noticeable clusters. We defined a scoring system based on the levels of expression of a list of progenitor and neuron-specific genes in each cell (see Methods). This system shows the highest progenitor (P) and neuron (N) scores at opposite ends of the UMAP representation, with intermediate values of both scores in between (Figure 1B), indicating that the progression from progenitor to neuron spontaneously emerges as a strong differentiating factor. Importantly, the expression of Btg2/Tis21 peaks in the region containing cells with intermediate values of both scores (Figure 1B) suggested that this region hosts neurogenic progenitors. This agrees with clonal analyses showing that proliferative and neurogenic stages correspond to successive steps of maturation of progenitors on the path to differentiation. We then refined this analysis through pseudo-temporal classification of these cells to identify gene clusters with similar transcriptomic profiles along the pseudo-time axis (Figure 1C). Interestingly, the gene cluster that

contained Tis21 also contained genes with known expression and/or functions at the transition from proliferation to differentiation, such as the Notch ligand Dll1, the bHLH transcription factors Hes6, NeuroG1 and NeuroG2, and the coactivator Gadd45g. We used this list of genes to define a "neurogenic progenitor" (PN) score (Figure 1D) and performed a differential expression analysis based on P, N and PN scores (Figure 1E). In addition to 5 of the 6 genes used to define the PN score itself, the list of 10 genes showing the most significant differential expression between PN and the other populations included a) three genes with unknown function in the neurogenic transition (ZC3H12C, LOC107051857, BAMBI), b) the centrosomal gene ninein (NIN), whose differential regulation at that stage has previously been described (Zhang et al., 2016), and c) the cell cycle regulator CDKN1c (Figure 1E).

2) scRNAseq analysis reveals the dynamics of CDKN1c expression during the neurogenic transition.

Cdkn1c (Cyclin-dependent Kinase inhibitor 1c) encoding the $p57^{KIP2}$ protein (Matsuoka et al., 1995) was one of the strong candidates to emerge from our analyses. In pseudotime analyses as well as on the UMAP visualization (Figure 1C, F), its expression profile is similar to that of Tis21, being expressed at low levels in the subset of the progenitor population that we interpret as "neurogenic". However, while Tis21 expression rapidly fades off, Cdkn1c transiently peaks at high levels slightly later before fading off in mature neurons. Most importantly, Cdkn1c is an inhibitor of Cyclin/CDK (Cyclin dependent kinase) complexes responsible for G1-phase progression and G1- to S-phase transition. During CNS development, gain and loss-of-function approaches have uncovered a role for Cdkn1c in cell cycle exit and neural differentiation both *in vitro* and *in vivo* (Gui et al., 2007; Tury et al., 2011). In the spinal cord of CDKN1c knock-out mice, a delay in neurogenesis was observed, mostly attributed to a reentry of nascent neurons in the cell cycle (Gui et al., 2007). Nonetheless, CDKN1c expression has been observed in some neural progenitors (Gui et al., 2007; Mairet-Coello et al., 2012a; Tury et al., 2011) and a shortening of G1-phase has been described in the CDKN1c knock-out mouse cortex (Mairet-Coello et al., 2012b). Interestingly, CDKN1c transcripts are specifically enriched in Tis21-positive progenitors in the mouse embryonic cortex (Arai et al., 2011) and our scRNAseq analyses show a similar upregulation in chick Tis21-positive neurogenic progenitors in the spinal cord. We therefore postulate that the progressive elevation of Cdkn1c levels in cycling progenitors first favors a transition from proliferative to neurogenic modes of division, before

higher levels of Cdkn1c in daughter cells fated to become neurons drive them to leave the cell cycle.

3) *CDKN1c*/p57Kip2 expression levels underlie different cellular states in the embryonic spinal cord

To test this hypothesis, we explored the dynamics of Cdkn1c expression by in situ hybridization in the chick embryonic spinal (Figure 2A) cord during the neurogenic transition. While CDKN1c was absent at E2, before neurogenesis really starts the transcript was detected at E3 and E4, when neurogenesis is well underway, underscored by the expression of HuC/D in the mantle zone (see lower panels of Figure 2A). It was expressed at low levels in a salt and pepper fashion in the ventricular zone, where the cell bodies of neural progenitors reside, and markedly increased in a domain immediately adjacent to this zone which is enriched in nascent neurons on their way to the mantle zone. In contrast, the transcript was completely excluded from the mantle zone, where HuC/D positive mature neurons accumulate. This is consistent with the dynamics of the in-silico profile described above.

We then checked whether the CDKN1c/p57kip2 protein is translated in the population of progenitors in which the CDKN1c transcript is detected. In the absence of antibodies functional in the chick embryo, we used a CRISPR/Cas9-based somatic knock-in strategy to insert an array of 6 Myc tags at the C-terminus of CDKN1c (Supplementary Figure 1A-B). The Myc tags insertion approach offers a direct read-out of the presence of the CDKN1c protein, and should report any cell cycle dependent stabilization or degradation of CDKN1c. The Myc tags were immediately followed by a P2A pseudo-cleavage site and the Gal4-VP16 transcription factor sequence (Supplementary Figure 1A-B). whose simultaneous translation can be used to activate the transcription of a stable reporter (eg. EGFP) from a UAS promoter. This allows to identify both Myc-CDKN1c-positive cells and cells in which Myc-CDKN1c is no longer present but has previously been expressed.

We electroporated the knock-in vector together with a plasmid expressing Cas9 and gRNAs targeting the CDKN1c C-terminus and a UAS-nls-EGFP reporter plasmid in the neural tube of E2 chick embryos At E3, we observed a strong GFP signal in the electroporated side of the embryo using three different CDKN1c gRNAS, whereas no signal was observed when a control

gRNA that does not target any chick sequence was used, indicating successful and specific knock-in events (Supplementary Figure 1C). Immunohistochemistry on transverse sections at E4 revealed low but detectable Myc signal in the ventricular zone, while a stronger signal was observed in the intermediate domain, and virtually no signal in the mantle zone (Figure 2B). This pattern is very similar to the expression of the transcript observed via in situ hybridization (Figure 2A). To ascertain that CDKN1c protein is present in cycling progenitors, we used anti-Myc antibody in combination with a pRb antibody, recognizing a phosphorylated form of the Retinoblastoma (Rb) protein). Although pRb is specific for cycling cells, it is only detected once cells have passed the point of restriction during the G1 phase.

We detected many double GFP+/pRb+ cells (arrows and arrowheads in Figure 2B) in the ventricular zone, indicating that the CDKN1c transcript is translated in cycling progenitors. Only a few GFP+/pRb+ cells were also Myc-positive (arrowheads in Figure 2B). This is consistent with a short period of overlap between CDKN1c protein and pRb around the timing of the restriction point, indicating that CDKN1c protein is degraded in later phases of the cell cycle. We also observed some weak Myc+ cells in the VZ that were also pRb-negative (asterisks, Figure 2B). This may correspond to the onset of CDKN1c expression in progenitors during early G1, before Rb phosphorylation. Alternatively, they might be early nascent neurons, whose nucleus is still located in the VZ, and about to upregulate their CDKN1c level and translocate basally (see Scheme Figure 2C). In line with this observation, we also observed many GFP+ nuclei with a strong Myc signal but without pRb-staining located in the intermediate domain, corresponding to nascent neurons in the process of exiting the cell cycle and on their way to differentiation (Figure 2B; double asterisks).

Importantly, these observations confirm that Cdkn1c protein is expressed at low level in a subset of progenitors in the chick spinal cord. Our knock-in strategy which reveals the history of CDKN1c transcription and translation suggests that the protein is quickly degraded during or after G1 completion, and may explain why only rare CDKN1c positive progenitors were observed with CDKN1c antibodies in previous studies. Indeed, this is consistent with data obtained in the mouse spinal cord at E11.5 (which corresponds approximately to E4 in chick embryo), where only a small number of cells expressing CDKN1c (p57) protein has been shown to co-express the progenitor marker Pax6 and to incorporate BrDU in the ventricular zone (Gui

et al., 2007). Similarly, a few mouse PCNA+ and Tbr2+ cortical progenitors coexpressed the CDKN1c ($p57^{kip2}$) protein (Gui et al., 2007; Mairet-Coello et al., 2012).

Altogether our scRNAseq analyses, in situ hybridization and knock-in experiments is consistent with our hypothesis of two sequential roles of CDKN1c in progenitors and neurons.

4) Downregulation of Cdkn1c in neural progenitors delays the transition from proliferative to neurogenic modes of division

We functionally investigated the specific role of Cdkn1c as a potential player in the transition between division modes. We chose to use a loss-of function strategy based on the short hair-pin RNA (shRNA) approach, with the rationale that a partial knock-down efficiency would be sufficient to delay the onset/increase of Cdkn1c expression. While this approach would result, in its complete absence from the progenitor population, it would not be sufficient to prevent cells from eventually reaching a level of Cdkn1c sufficient to trigger cell cycle exit. Of the six shRNA that were tested against Cdkn1c (see Methods), only two (sh1 and sh4) induced a reduction of Cdkn1c mRNA expression that was consistently observable on transverse section, while an effect the other four was not clearly visible (Supplementary Figure 2A).

We first investigated the effect of this modest Cdkn1c knock-down on the production of neurons at the tissue level. In order to target and investigate specifically the neurogenic switch, we concentrated our analyses on the dorsal region where the neurogenic transition has barely started at the time of electroporation of the shRNA vectors (E2.25, HH13-14). Neuron and progenitor populations were evaluated 24 or 48 hours after electroporation (hae) via immunohistochemistry (see Methods for the choice of the markers of these populations).

shRNA1 and shRNA4 led to a significant increase in the number of pRb-positive progenitors 48 hae (Figure 3B and Supplementary Figure 2B). Accordingly, the neuron population, identified with HuC/D, was decreased 48h after Cdkn1c knock-down by shRNA1 (Figure 3B). This switch towards proliferation was already apparent 24 hours after shRNA electroporation, as illustrated by a modest but significant increase in the pRb+ progenitor population in shRNA1 condition (Figure 3A). We further assessed that the reduction in neuronal production was not due to cell death, as we observed no excess in the number of Caspase3-positive cells in the knock-

down condition (data not shown). The following experiments were carried out using shRNA1 (called shRNA Cdkn1c thereafter) which showed the most efficient downregulation in *Cdkn1c* expression and the most significant dysregulation in the ratio of progenitor versus neuron populations in our functional studies.

We postulated that the observed reduction in neurogenesis may result from a delay in the transition from proliferative to neurogenic modes of division, rather than the proposed failure of prospective neurons to exit the cell cycle (Gui et al., 2007). To more directly address this hypothesis, we developed a clonal analysis strategy to analyze the fate of pairs of sister cells whose mothers were downregulated for Cdkn1c (Figure 3D). This approach will allow to retrospectively deduce the mode of division used by the mother progenitor cell. To do so, we used the cell permeant dye "FlashTag" (FT) to specifically label a cohort of progenitors that undergoes mitosis synchronously in a +/- 30-minute time period after FT injection in the neural tube (Baek et al., 2018b; Telley et al., 2016) and Methods). We first established that within pairs of cells labelled by FT, the sister cell(s) that reenter the cell cycle have crossed the restriction point within a six hours time-window after injection of the dye at E3, and are therefore reliably identified as progenitors thanks to pRb positivity. On the contrary, the FT positive sister cell(s) that are pRb-negative are considered as neural precursors on their way to differentiation. Two-cell clones selected on the basis of FT incorporation can therefore be categorized as PP, PN, or NN based on pRb positivity (P) or not (N) (see Methods and Supplementary Figure 3A-B). We characterized pairs of GFP+/FT+ sister cells born from control versus progenitors electroporated with the CDKN1c shRNA at E2.25 and injected one day later with FT (Figure 3D-E). Strikingly, we observed a massive increase in the number of PP clones at the expense of PN and NN clones, indicating a shift towards a proliferative mode of division in the CDKN1c-downregulated condition (Figure 3F). In agreement with this observation, analysis of pairs of sister cells upon KI of the Gal4 driver in the CDKN1c locus showed a significantly higher proportion of neurogenic (PN and NN) pairs born from CDKN1c-positive progenitors compared to the total progenitor population (Supplementary Fig3C).

Altogether, our loss-of-function analyses at the tissue and at the single progenitor level suggest that CDKN1c expression in progenitors at E3 regulates the balance between proliferative and neurogenic modes of division.

5) Inducing a premature expression of CDKN1c in progenitors triggers the transition to neurogenic modes of division

Our expression studies and knock-down experiments indicate that CDKN1c is already active in a subset of progenitors, and that it is necessary to initiate the neurogenic process. To explore whether it is sufficient to induce the neurogenic transition, we sought to induce premature expression of CDKN1c in proliferative progenitors. To avoid the cell cycle arrest that is triggered in progenitors by strong overexpression of CDKN1c (Gui et al., 2007), we aimed to mimic the modest level of expression observed in neurogenic progenitors and to restrict this overexpression to cycling cells. We therefore decided to introduce the coding sequence of CDKN1c in the Pax7 locus, whose expression is restricted to progenitors in the dorsal domain, with the expectation that:

1) this would lead to a premature expression of CDKN1c in the proliferative dorsal precursors, at a level similar to that observed in the neurogenic precursors (as suggested by the levels of CDKN1c and Pax7 expression in our scRNAseq data – Supplementary Figure 4A), but without reaching the endogenous level of expression observed in the nascent neurons.

2) this expression would be transient and switched off in nascent neurons.

We used the CRISPR/Cas9-based somatic approach to introduce a 3xMyc-tagged CDKN1c coding sequence and the Gal4-VP16 transcription factor downstream of Pax7 (Figure 4A, Supplementary Figure 4B-C and methods).

Embryos at E2.25 were electroporated with this construct, in combination with a plasmid coding for Cas9 and a gRNA targeting Pax7 C-terminus, and an UAS-nls-EGFP reporter plasmid. A strong GFP signal was observed 24 hours after electroporation when using the Pax7 gRNA, whereas no signal was observed using a control gRNA (Supplementary Figure 4D). To validate our approach, we used bilateral electroporation (Figure 4B) to compare the level of Pax7-driven overexpression of CDKN1c on one side of the neural tube to the endogenous level of CDKN1c on the contralateral side. Immunohistochemistry on transverse sections at E3 and E4 confirmed that the Myc signal resulting from CDKN1c-Myc expression from the Pax7 locus was restricted to progenitors, at a level similar to that observed for endogenous Myc-tagged

CDKN1c in progenitors. Importantly, the signal remained below the endogenous level of Myc-tagged CDKN1c observed in nascent neurons, thus fulfilling all the criteria listed above (Figure 4B and Supplementary Figure 4E).

We therefore proceeded to the analysis of CDKN1c overexpression in progenitors. At the population level, at E4, the premature CDKN1c expression from the Pax7 locus resulted in a strong reduction in the number of progenitors (pRb positive cells) within the knock-in population (UAS-nls-GFP reporter positive cells), matched by a significant increase in the proportion of neurons (HuC/D+) (Figure 4C), indicating an increase in neurogenesis 48 hours after electroporation.

We next examined the mode of division of progenitors overexpressing CDKN1c. Using the FlashTag cohort labeling approach described above, we traced the fate of daughter cells born 24 hours after electroporation. We observed a massive increase in the proportion of neurogenic divisions (from 28% to 40%, for PN pairs and from 10% to 43% for NN pairs) at the expense of proliferative pairs (PP pairs; 17% in overexpressing cells vs 62% in controls) (Figure 4D). Overall, these data show that forcing CDKN1c expression at low-level in cycling progenitors accelerates the transition towards neurogenic modes of division.

6) Cdkn1c modulates cell cycle parameters in neural progenitors.

Previous data in the developing cortex of CDKN1c knock-out mice described a transient increase in proliferation (between E14.5 and E16.5) linked to a shorter progenitor cell cycle duration mainly due to a reduction of the G1 phase length (Mairet-Coello et al., 2012). However, in addition to its role as a cell cycle regulator, Cdkn1c also performs other functions, as illustrated by its role as a transcription co-factor or pro- or anti-apoptotic factor in different contexts (Creff and Besson, 2020).

To assess the mechanisms of action of Cdkn1c in the neurogenic transition, we monitored cell cycle parameters in reduced Cdkn1c conditions (see Methods). Cumulative EdU incorporation in spinal progenitors (pRb+) at E3 (24hae) showed that the proportion of EdU-positive progenitors reached a plateau faster and in a sharper manner in the Cdkn1c shRNA population (Figure 5A-B). This indicates that the total duration of the cell cycle is shorter upon Cdkn1c knockdown. To specifically assess a possible reduction in G1 length, we developed an approach that

provides a direct measurement of G1 duration, contrary to the classical method of G1 inference described by (Nowakowski et al., 1989). Our approach uses precise landmarks to delineate G1 phase borders: mitosis exit (through the Flash Tag labeling of a synchronized cohort of dividing progenitors) and S-phase entry (through cumulative EdU labeling; Figure 5C, see Methods). We found that the proportion of pRb+ progenitors having entered S phase (EdU+ cells) was higher at all time points examined after FT injection in the Cdkn1c knock-down condition compared to the control population (Figure 5D). Importantly, virtually all progenitors electroporated with shRNA had reached S-phase 10h30 after FT injection, while around 1/3rd of control progenitors were still in G1 at that time. Taken together, these results demonstrated a shorter cell cycle in Cdkn1c-downregulated condition at the population scale, which is, at least partially, related to a decrease in G1 duration.

7) Restoring cell cycle parameters rescues the CDKN1c downregulation effect on neurogenesis

We next explored whether these changes in cell cycle parameters could explain the decrease in neuron production observed upon CDKN1c knock-down. For this, we functionally challenged CyclinD1, a major target of Cdkn1c which has opposite effects on G1 phase duration and cell cycle exit (Gui et al., 2007). Cyclin D1 acts during G1 to promote proliferation. In accordance, its loss of function by shRNA reduces the number of cycling cells in the chick embryonic neural tube (Lacomme et al., 2012; Lukaszewicz and Anderson, 2011) and favors neurogenesis in the mouse cortex, possibly through a lengthening of G1 phase (Lange et al., 2009) . We therefore hypothesized that a concomitant downregulation of CyclinD1 should rescue, at least partially, the anti-neurogenic phenotype observed with a Cdkn1c downregulation alone.

We validated that a published shRNA targeting chick Cyclin D1 (Lukaszewicz and Anderson, 2011) led to its efficient downregulation (Supplementary Figure 5). We then evaluated the effect of the simultaneous downregulation of CyclinD1 and CDKN1c. Remarkably, at 48hae, whereas Cdkn1c shRNA and CyclinD1 shRNA alone respectively increased and decreased the proportion of EdU positivity in progenitors, the double Cdkn1c/CyclinD1 knock-down was undistinguishable from control, (Figure 5E). This recovery of control levels in the double knock-down condition is consistent with Cdkn1c and CyclinD1 having opposite effects on G1 duration.

We then analyzed the fate of pairs of sister cells born from progenitors dividing 24 hours after electroporation in these four conditions. At that stage, when CDKN1c knock-down leads to a shift towards more PP divisions, as described above, CyclinD1 knock-down alone did not alter the distribution of PP, PN and NN pairs compared to the control situation. However, in the double knock-down experiments, the anti-neurogenic effect of Cdkn1c knock-down was counteracted by the downregulation of CyclinD1 (Figure 5F). Consistently, at the population level at E4, CyclinD1 downregulation fully rescued the Cdkn1c knockdown phenotype and restored the rate of neurogenesis to that of a control situation whereas its sole downregulation did not affect the ratio of proliferating progenitors and neuron production 48hae (Figure 5G).

These results demonstrate that reducing CyclinD1 expression efficiently counteracts the phenotype observed upon Cdkn1c downregulation, both at the population scale and at the level of individual progenitors, suggesting that this phenotype is largely resulting from an effect on CyclinD1/CDK6 regulation of cell cycle dynamics.

Our detailed description of the dynamics of CDKN1C expression during spinal cord neurogenesis establishes that it is turned on at low level in neurogenic progenitors before it peaks at high expression level in future neurons. Specifically modulating this early phase of expression via loss or gain and function impairs the balance between proliferative and neurogenic modes of division. Overall, this study uncovers an underestimated role for CDKN1c/p57^{kip2} activity favoring the neurogenic transition in progenitors.

DISCUSSION

In this report, we used scRNAseq data generated from the chick cervical spinal cord to identify regulators of the neurogenic transition. We used a pseudotime reconstitution to order cycling progenitors along the sequence of proliferative to neurogenic modes of division. Using a set of genes that clustered with the neurogenic marker Tis21 in this analysis, we established a "neurogenic progenitor score" that was used for differential expression analyses. We focused on one of the most significant candidates emerging from this analysis, the CDK/Cyclin inhibitor CDKN1c. Our functional analyses allow us to re-interpret its role during spinal neurogenesis, and show that it is more than a binary regulator of cell cycle exit: we demonstrate that Cdkn1c is also an intrinsic regulator of the neurogenic transition through a change in the mode of division of progenitors, acting primarily via the inhibition of the CDK6/CyclinD1 complex.

Cell cycle regulators are key players in the process of differentiation. One obvious role is to control the cell cycle exit in neuron precursors that are fated to differentiate. Studies in a wide range of species have also demonstrated that cell cycle regulation is already involved at the level of cycling progenitors of the developing CNS for the commitment of their progeny to a neural fate (Calegari and Huttner, 2003; FUJITA, 1962; Kicheva et al., 2014; Lange et al., 2009; Lukaszewicz and Anderson, 2011a; Pilaz et al., 2009; Smith and Schoenwolf, 1987; Takahashi et al., 1995). Among the different parameters of the cycle, a change in the duration of G1 phase in the dividing mother cell, in absolute or relative terms in relation to the duration of the cycle, is crucial to modulate the capacity of the daughter cells to self-renew or differentiate (Calegari and Huttner, 2003; Lange et al., 2009; Pilaz et al., 2009). Consistent with this idea, Tis21 positive neurogenic progenitors display a longer G1 phase (absolute or relative to the duration of the cell cycle) compared to Tis21 negative proliferative progenitors in the developing mouse cortex (Calegari et al., 2005; Calegari and Huttner, 2003; Lange et al., 2009). A lengthening of the G1 phase is observed during the transition from aRG to fate restricted progenitors (BiP) (Arai et al., 2011), and live imaging has demonstrated a lengthening of the G1 phase between two consecutive cycles in the chick spinal cord (ref Molina). Functional explorations of the role of G1 length on the mode of division have mostly focused on Cyclin/CDK complexes (Calegari et al., 2005; Calegari and Huttner, 2003; Lange et al., 2009; Pilaz et al.,

2009). Intriguingly, while Cdkn1c is a key regulator of Cyclin/CDK complexes that control G1 length, its gain and loss of function phenotypes in the CNS have essentially been attributed to a post mitotic role in daughter cells, primarily through its function in regulating cell cycle exit (Gui et al., 2007; Mairet-Coello et al., 2012; Tury et al., 2011). Our study combines a detailed analysis of CDKN1c expression dynamics in progenitors and nascent neurons with functional approaches specifically targeting its activity in progenitors to resolve this apparent paradox. Using an innovative somatic knock-in strategy, we were able to tag the CDKN1c locus with Myc epitopes and access to the history of CDKN1c transcription and translation via the Gal4-UAS reporter. Using clonal analyses, we were able to infer with a cellular resolution the mode of division of individual progenitors from the fate of their daughters and we showed that reducing CDKN1c expression in progenitors favors a proliferative mode of division and eventually impedes neurogenesis. Conversely, we show that a premature overexpression of CDKN1c restricted to cycling cells is sufficient to convert proliferative into neurogenic progenitors. In addition, we have clarified the cellular mechanisms of Cdkn1c in this phenotype and proposed that Cdkn1c also regulates the switch to a neurogenic division mode mainly through an elongation of the G1 phase of the cell cycle resulting from the inhibition of the CyclinD/CDK6 complex.

Taken together, our study adds a new player in the complex panorama linking cycle dynamics and progenitor cell behavior. It reinforces the view that a faster or slower passage through the G1 phase of a progenitor is instructive for its proliferative versus neurogenic mitotic behavior, and therefore dictate the fate of its daughters.

What regulates CDKN1c expression in progenitors? Gui et al proposed that the strong upregulation of CDKN1c that is required to drive prospective neurons out of the cell cycle is under transcriptional control of the NeuroG2 transcription factor in the spinal cord (Gui et al., 2007). Indeed, a massive overexpression of NeuroG2 leads to a strong CDKN1c upregulation and cell cycle exit. However, the analysis of our scRNAseq dataset showed that NeuroG2 is also expressed at low levels in neurogenic progenitors (Figure 1D) and could therefore act upstream of CDKN1c onset in progenitors. On the other hand, NeuroG2 protein stability and activity is controlled by the CDKN1c homolog p27Kip1/CDKN1b (Nguyen et al., 2006). Whether CDKN1c has a similar effect on NeuroG2 activity has not been tested directly, but it is tempting to

speculate that CDKN1c and NeuroG2 might be involved in a positive feedback loop progressively leading from their moderate expression causing G1 lengthening in neurogenic progenitors to a peak of expression driving cell cycle exit in prospective neurons. Consistent with this scenario, NeuroG2 is also involved in the downregulation of cyclinD1 and cyclinE2 in spinal progenitors (Lacomme et al., 2012). Additionally, or alternatively, CDKN1c expression may be controlled by a regulatory cascade involving the HES genes. It has been shown in pancreatic progenitors that CDKN1c is transcriptionally repressed by HES1, downstream of the Notch pathway (Georgia et al., 2006) and the same authors report a complementary expression of Hes1 and CDKN1c in the mouse neural tube. Our scRNASeq data analysis confirms a similar complementarity between HES5 (which appears to be the main HES factor in the chick spinal cord (Fior and Henrique, 2005) and CDKN1c. The transcriptional activity of Hes1 in pancreatic progenitors is repressed by Hes6. Interestingly, the onset of expression of HES6 shortly precedes that of CDKN1c in the chick embryonic spinal cord scRNASeq dataset. This suggests that the initiation of CDKN1c expression in neurogenic progenitors might be triggered by the antagonistic activity of HES6 on HES1/HES5. Further work is needed to decipher the mutual relationships regulating the dynamic expression of these factors during the neurogenic transition.

All the proposed candidates display dynamic expression during the process of neurogenesis, and different levels in their expression may correspond to different activities at different cellular states, as illustrated in this study with CDKN1c. This renders difficult to disentangle their multiple functions via complete loss-of-function or massive overexpression. Here, we circumvented these limitations via a simple and efficient somatic knock-in method that allowed us to tightly control the level and duration of exogenous overexpression of CDKN1c in a subset of progenitors in the chick embryo. The knowledge of the diverse timings and levels of expression of large panels of genes from scRNAseq analyses opens the way to generalize similar customized approaches for further functional exploration of regulatory networks during neurogenesis. This strategy could also be extended to other contexts and animal models, enabling to bypass the lengthy process of transgenic line generation and complex crossing schemes.

One key aspect of the neurogenic transition is the reliance on asymmetric division in the early stages of neuron production. Asymmetric division of neural progenitors is an active process

relying on intrinsic asymmetries in the progenitor cell involving the unequal distribution of fate determinants during mitosis (eg. Tozer 2017, Saade 2017, papiers Sara 10.1038/ncb3119 …). It will be important to understand whether and how CDKN1c and other regulators of the cell cycle are involved in setting up the intrinsic polarities necessary for this process in neural progenitors. In this context, it is interesting to note that cell cycle regulators have already been shown to play a direct role in the machinery that establishes cellular asymmetry during the division of drosophila neuroblasts (Tio et al., 2001) and sensory organ precursors (Darnat et al., 2022); on the other hand, studies in the developing mouse cortex have shown that the cyclinD2 mRNA is asymmetrically localized and inherited upon division of neural progenitors, and behaves as a fate determinant in their progeny (Tsunekawa et al., 2012). Hence, cell cycle regulators are likely to be involved at multiple levels in the process of neurogenesis, from the determination of the neurogenic competence of neural progenitors to the cellular process of asymmetric division. In this context, it will be interesting to explore whether and how Cdkn1c controls the asymmetric distribution of fate determinants that have been identified over the last years (Peyre and Morin, 2012; Saade et al., 2017; Tozer et al., 2017; Tsunekawa et al., 2012).

MATERIALS AND METHODS

A. Transcriptomic analysis

Production of scRNA-seq data

Sample preparation of chick cervical progenitors for single-cell RNA sequencing.

Three chick embryos at 66 hours of embryonic development were collected and dissected in ice-cold 1x Phosphate Buffered Saline solution (PBS), transferred into ice-cold L15 medium for further dissection to retain only the cervical spinal region (spanning the length of 5 somites starting from somite n°8). To generate a single-cell suspension, dissection products were then transferred in 250µl of 37°C pre-heated papain/L15 solution (Worthington, REF: LS003126 – Stock solution = 41,6mg/ml in 100ml; Working solution = 50µl of stock solution diluted in 1,5ml of L15 medium) and incubated at 37°C for 15 minutes. Papain was then replaced with ice-cold L15 medium, and clusters of cells were disaggregated through gentle up-and-down pipetting. Cells were then centrifuged at 300g for 2 minutes at 4°C. The supernatant was removed, and 500µl of new ice-cold L15 medium was added. Another round of up-and-down pipetting was performed, and cells were then sieved through 30µm filters to eliminate clumps of poorly-dissociated cells. Filtered cells were then centrifuged for 4 minutes at 300g, and the supernatant was replaced with 1ml of PBS containing 0.04% BSA. Cells were then centrifuged for 4 minutes at 300g, 900µl of supernatant was removed and cells were then re-suspended in the remaining 100µl of solution. Quality control was assayed by counting live vs dead cells using Trypan blue. Samples with >90% viability were then used for the generation of scRNAseq datasets. After viability assessment, cell concentration of samples was adjusted to 1000cells/µl.

Single cell transcriptomes generation, cDNA synthesis and library construction.

Single-cell RNA-seq and Illumina sequencing were performed at the Ecole Normale Supérieure GenomiqueENS core facility (Paris, France). The cellular suspension (4000 cells) was loaded on 10x Chromium instrument to generate 2871 single-cell GEMs, using the manufacter's instructions (single cell 3’ v2 protocol, 10x Genomics). Library construction was performed as per the manufacturer’s protocol and then sequenced on a NextSeq 500 device (Illumina) using paired-end (PE) 26/57, generating 533 million reads.

Pre-processing of chick scRNA-seq data.

Primary analyses (demultiplexing, UMI processing, mapping, feature assignment and gene quantification) were performed with Eoulsan 2 (Lehmann et al., 2021). We used as references the NCBI chick reference genome assembly galGal6.fa.gz and a dedicated GTF annotation scAnnotatiONT_isoquant.gtf. This annotation was built on top of the NCBI galGal6.ncbi-RefSeq.gtf.gz annotation (downloaded from https://hgdownload.soe.ucsc.edu/goldenPath/galGal6/bigZips/genes/). Due to the high number of poorly annotated genes' 3'UTRs in the chick genome, we developed a novel approach based on the re-annotation of the genome with single-cell RNA-seq data (10x Genomics short reads) and long reads bulk RNA-seq (Oxford Nanopore Technologies) from the same cell types in the chicken embryo. We also developed an open-source pipeline written in Nextflow, scAnnotatiONT, which supports this approach (Lehmann et al, manuscript in preparation). This pipeline mainly relies on the use of the genome-based analysis tool IsoQuant (Prjibelski et al., 2023) for the transcript reconstruction step. We also added filtering and quality checks of the novel annotation based on the single-cell RNA seq data.

Biological analyses of scRNA-seq data

Data cleaning and preparation.

The chick dataset was subjected to cleaning steps before proceeding with analyses. Filtering was performed to remove unwanted cells: cells presenting UMI counts below the 0.5th percentile and above the 99.9th percentile, more 20% UMI counts associated with mitochondrial genes and more than 0.3% UMI counts associated with hemoglobin genes. This filtered dataset contained 2479 cells. With regard to gene filtering, we kept genes that are expressed at least once in at least 3 cells. All filtering analyses were performed using Seurat v3.

Normalization and dimension reduction.

Data were log-normalized with Seurat v3 function "NormalizeData", and confounding factors such as cell cycle phases and gender were then regressed out using the function "ScaleData"

(Lehmann et al., 2021). To preserve differences between proliferating and non-proliferating cells, we separated cells in two groups: “cycling” (G2/M and S) and “non-cycling” (G1/G0). Dimension reduction was then performed on scaled data, and 2D representation of the dataset (PCA & UMAP plots) were obtained. After consulting the percentage of variance explained by each dimension, we chose to keep the first 30 components.

Cell classification.

First, using the expression of known cell population markers, we removed all cells that were neither progenitors or neurons such as cells of the mesoderm (expressing Foxc1/2, Twist1/2, Meox1/2, Myog10) and neural crest (expressing Sox10) as performed in (Delile et al., 2019). At this stage, 1878 chick cells remained. To better characterize these neural cells, we applied self-defined progenitor (P) and neuron (N) signature scores, using the Seurat function “AddModuleScore”. Scores were based on several known and newly-identified markers (originating from differential analysis performed in an initial dataset exploration). Detailed list of used marker genes is provided below.

(Progenitor genes = Sox2, Notch1, Rrm2, Hmgb2, Cenpa, Ube2c, Hes5; Neuron genes = Tubb3, Stmn2, Stmn3, Nova1, Rtn1, Mapt)

Clustering and differential expression.

In order to identify sub-populations of cells within the population of interest, we then performed graph-based clustering using the Louvain algorithm as implemented in Seurat v3. Clustering, coupled with differential expression results (obtained using a negative binomial test) did not bring out clusters evocative of a delineation between proliferative and neurogenic progenitor populations, as cells were mainly differentiated by the patterning factors of the dorso-ventral (DV) axis. In order to find other variation sources, we designed a “denoising” strategy based on pseudotime analysis.

Pseudotime analysis.

The pseudotime analysis was performed on the whole neural population. In order to identify genes whose expression varies over time, we relied on the “DifferentialGeneTest” function of the trajectory-inference dedicated tool Monocle3, which led to hierarchical clustering of

genes along a pseudotime axis. Partitioning around medoids algorithm (PAM) was then applied to cluster cells based on similar gene expression profiles along the pseudotime. We then focused on the Btg2/Tis21-containing cluster to look for differentially-expressed genes (Figure 1C).

B. Experimental Model

Fertilized eggs of JA57 chicken were purchased from EARL Morizeau (8 rue du Moulin, 28190 Dangers, France). Eggs were incubated at 38°C in a Sanyo MIR-253 incubator for the appropriate amount of time.

Cryostat sections

For cryostat sections, chick embryos were collected at E2.25 (HH st13-14), E3 (HH st18) and E4 (HH st22) (Hamburger and Hamilton, 1992) in ice-cold PBS, then fixed over-night in 4% formaldehyde/PBS at 4°C. The following day, embryos were washed 3 times for 5 minutes in PBS at room temperature (RT). Embryos were equilibrated at 4°C in PBS/15% sucrose, then equilibrated at 42°C in PBS/15% sucrose/7,5% gelatin solution, embedded in plastic dishes containing 1mL of PBS/15% sucrose/7,5% gelatin solution and flash frozen in 100% ethanol at -50°C on dry ice, before storage at -80°C. Prior to cryostat sectioning, samples were equilibrated for 1 hour at -25°C. 20µm cryostat sections were obtained using a Leica CM3050 S Cryostat and manually mounted on SuperFrost Plus microscope slides, before storage at -20°C.

In Situ Hybridization

For in Situ Hybridization, gelatin-mounted cryosections were first equilibrated at room temperature for 15 minutes, and de-gelatinized by washing slides in 37°C PBS 3 times for 5 minutes. All following steps were carried at RT unless mentioned otherwise. Slides were bathed for 20 minutes in RIPA buffer (150mM NaCl, 1% NP-40, 0.5% Na deoxycholate, 0.1% SDS, 1mM EDTA, 50mM Tris pH 8.0), post-fixed in 4% paraformaldehyde/PBS for 10 minutes, and washed with PBS 3 times for 5 minutes. Slides were then bathed in Triethanolamine solution (100mM triethanolamine, acetic acid 0.25% pH 8.0) for 15 minutes and washed with PBS 3 times for 5 minutes. Subsequently, slides were pre-hybridized during 1 hour in 69°C pre-

heated hybridization solution (50% formamide, 5X SSC, 5X Denhardt's, 500 µg/mL herring sperm DNA, 250 µg/mL yeast RNA) and hybridized overnight at 69°C with the same hybridization solution in presence of the heat-denatured (95°C for 5 minutes) DIG-labelled RNA probes. The following day, slides were transferred in post-hybridization solution (50% formamide; 2x SSC; 0.1% Tween20) at 69°C for 1 hour, then washed in 69°C pre-heated 2x SSC solution for 30 minutes, and finally in 0.2x SSC solution at RT for 5 minutes. Slides were washed with buffer 1 (100mM maleic acid, pH 7.5, 150mM NaCl, 0.05% Tween 20) during 20 minutes at RT, blocked for 30 minutes in buffer 2 (buffer 1/10% FCS), followed by overnight incubation at 4°C with 250µl of the anti-DIG antibody (Merck #11093274910 - diluted 1:2000) and other necessary primary antibodies (when additional immunostaining was needed) in buffer 2. Slides were covered with a coverslip to limit loss of solution during overnight incubation. The following day, coverslips were gently removed and slides were washed with buffer 1, 3 times for 5 minutes, and equilibrated for 30 minutes by bathing in buffer 3 (100mM Tris pH 9.5, 100mM NaCl, 50mM MgCl2). In Situ Hybridization signal was visualized through a colour reaction by bathing slides in BM-Purple (Merck # 11442074001). The colour reaction was allowed to develop in the dark at room temperature during the appropriate amount of time and was stopped by bathing slides in 4% paraformaldehyde/PBS for 10 minutes. Sections were finally washed with PBS 3 times for 5 minutes before either mounting with coverslip using Aquatex or proceeding with the subsequent immunostaining protocol steps if required (see section Vibratome / Cryostat sections and Immunostaining).

All of RNA-probes were synthesized using a DIG RNA labelling kit (Merck #11277073910) following manufacturer's protocol. Antisense probes were prepared from the following linearized plasmids: cHes5.1 (previously described in (Baek et al., 2018a), cCDKN1C (a gift from Matthew Towers, described in Pickering et al., 2019), and cCCND1 5'(a gift from Fabienne Pituello, previously described in (Lobjois et al., 2004).

In ovo electroporation

Electroporations were performed at HH13-14 by applying 5 pulses of 25V for 50ms, with 100ms in between pulses. Electroporations were performed using a square wave electroporator (Nepa Gene CUY21SC Square Wave Electroporator, or BTX ECM-830 Electro Square Porator, or Ovodyne Intracell TSS20) and a pair of 5 mm Gold plated electrodes (BTX

Genetrode model 512) separated by a 4 mm interval. For bilateral electroporation of the CDKN1C-Myc and Pax7-CDKN1c-Myc knock-in constructs (Figure 6), the two injections were performed at 3 hours interval, the polarity of the electrode was reversed and either 5 pulses of 25V (Supplementary Fig 2B) or 4 pulses of 20V (Fig2, Supplementary Figure 1) were applied for each electroporation.

Plasmids

RNA interference:

small interfering RNA sequences against the chick version of CDKN1C (cCDKN1C) were determined using siDirect: http://sidirect2.rnai.jp/. Target sequences for cCDKN1C are as follow:

cCDKN1C shRNA 1: 5' cggcaccgtgcccgcgttcta 3';

cCDKN1C shRNA 2: 5' cacgacccgcatcacagattt 3';

cCDKN1C shRNA 3: 5' agcgccgtctgcaggagctta 3';

cCDKN1C shRNA 4: 5' tgagccgggagaaccgcgccg 3';

cCDKN1C shRNA 5: 5'cgacccgcatcacagatttct 3'

cCDKN1C shRNA 6: 5' ctcaataaacaaaacaaaaaa 3'

Target sequences were cloned into the first hairpin of the miR30-derived structure of the pTol2-H2B-EGFP-miRNA plasmid (Peyre et al., 2011) using the following method (Das et al., 2006): 100ng of both General oligonucleotides (First hairpin primer 5': 5'-ggcggggctagctggagaagatgccttccggagaggtgctgctgagcg-3' and First hairpin primer 3': 5'- gggtggacgcgtaagaggggaagaaagcttctaaccccgctattcaccaccactaggca-3') were used together with 10ng of both target-specific oligonucleotides (Target forward sequence: 5'-gagaggtgctgctgagcgTARGETSEQUENCEtagtgaagccacagatgta-3' and Target reverse sequence: 5'-attcaccaccactaggcaTARGETSEQUENCEtacatctgtggcttcact-3') in a one-step PCR reaction to generate a product containing the miR30 like hairpin and the chick miRNA flanking sequences. Obtained PCR products and the pTol2-H2B-EGFP-miRNA plasmid were submitted to NheI/MluI double

enzymatic digestion, and purified digested products were then ligated to create CDKN1C miRNA plasmids.

The cCCND1 shRNA plasmid was previously described in (Lukaszewicz and Anderson, 2011), and was a kind gift of Dr Fabienne Pituello. A plasmid coding for a combination of a shRNA against Luciferase and a GFP reporter was used as a control (described in (Peyre et al., 2011). An empty pCAGGS plasmid was used to match total DNA concentrations between experimental and control electroporation mixes when needed. All miRNA and shRNA plasmids were used at 1 µg/µL except when otherwise mentioned.

Somatic knock-ins:

Somatic knock-in of a 6xMyc-P2A-Gal4-VP16 reporter at the C-terminus of the CDKN1c locus was achieved via CRISPR-Cas9-based microhomology-mediated end joining (MMEJ). The 6xMyc-P2A-Gal4-VP16 cassette in the targeting vector is flanked by 37bp 5' and 42bp 3' arms of homology corresponding to the genomic sequence immediately upstream and downstream of the stop codon of the CDKN1c locus. These arms of homology are flanked on both ends by a universal "uni2" gRNA target site that does not target any sequence in the chick genome (GGGAGGCGTTCGGGCCACAG; (Welker et al., 2021); Petit-Vargas et al, in prep). Details of the construct and cloning steps are available upon request. The MMEJ-based knock-in method relies on the simultaneous linearization of the target locus and of the targeting vector in cells. This is achieved by coexpression of two gRNAs, one targeting the genomic locus, the other (uni2) targeting the knock-in vector. We generated a double gRNA construct that possesses two cassettes, each expressing a chimeric gRNA under control of the human U6 promoter. This vector, derived from pX330 (Cong et al., 2013); Addgene #42230), also expressed humanized spCas9 protein under the CBh promoter. We chose 3 different gRNAs located in the vicinity of the CDKN1c stop codon, using the CRISPOR website (http://crispor.tefor.net/crispor.py). The sequence targeted by gRNA#1 (CTGAGCACACCCCCCGCAAG) is located 12 bases upstream of the CDKN1c stop codon in the sense direction and entirely comprised in the left arm of homology. In order to avoid targeting of the knock-in vector and of the modified locus after insertion of the knock-in cassette, the target sequence for gRNA#1 was destroyed in the left arm of homology via two conservative base changes in the last base of the recognition and in the PAM (see Supplementary Figure 1). Upon initial validation of the KI efficiency with a UAS-

nls-GFP reporter, gRNA#1 yielded the strongest GFP signal of the 3 gRNAs and was chosen for all subsequent experiments.

Somatic Knock-in of the CDKN1c coding sequence in the Pax7 locus was achieved via CRISPR-Cas9-based Homology-Directed Recombination (HDR). A Pax7-P2A-Gal4 knock-in vector and gRNAs were first generated and validated for efficient and specific targeting at the C-terminus of the Pax7 locus (not shown, described in Petit-Vargas et al, in preparation). In this vector, the Gal4-VP16 cassette is flanked with long left (1056bp) and right (936bp) arms of homology to the C-terminal region of Pax7. This vector was then modified by inserting a 846bp synthetic DNA fragment (IDT) coding for a P2A sequence, chick CDKN1c and 3 Myc tags, immediately downstream of the Gal4-VP16 sequence. This places a P2A-Gal4-VP16-P2A-CDKN1c-3xMyc cassette in frame with the C-terminus of Pax7. The introduction of two P2A pseudo-cleavage sequences ensures that Pax7, Gal4-VP16 and CDKN1c-Myc are produced as three independent proteins from the Pax7 locus in dorsal progenitors that have undergone homologous recombination. The Pax7 gRNA targets the GGGCTCCTACCAGTAGAGAC sequence 16 bases upstream of the Pax7 stop codon in the sense direction, and is entirely comprised upstream of the stop codon. In order to avoid targeting of the knock-in plasmid and re-targeting of the locus after insertion of the knock-in cassette, the gRNA target sequence was destroyed in the left arm of homology via insertion of 3 bases (AGA) 2 bases upstream of the PAM. This inserts an Arginine 5 amino acids upstream of the C-terminus of Pax7 (see Supplementary Figure 4C). In addition to this extra amino acid, a P2A sequence is appended at the C-terminus of the Pax7 protein expressed from the modified. We did not attempt to monitor whether this modification of the Pax7 C-terminus modifies its activity.

A gRNA that does not target any sequence in the chick genome was used as a control (GCACTGCTACGATCTACACC; (Gandhi et al., 2017)); For in ovo KI experiments, the homologous recombination and gRNA vectors were each used at 0.8µg/µl. The UAS reporter plasmid (pUAS-nls-EGFP) was added to the electroporation mix at 0.3µg/µl.

Vibratome sections

For vibratome sections, chick embryos were collected at desired stages and roughly dissected (to remove membranes) in ice-cold PBS, fixed for 1 hour in ice-cold 4% formaldehyde/PBS,

and rinsed 3 times for 5 minutes in PBS at room temperature (RT). Chick embryos were then finely dissected in PBS and subsequently embedded in 4% agarose (4g of agarose in 100ml of water, boiled in microwave and cooled at 50°C) until agarose became solid. Thereafter, 100 µm vibratome sections were realised using a ThermoScientific HM 650 V Microtome and collected in 6-well plates filled with cold PBS.

Immunostaining

Sections were permeabilized in PBS-0,3% Triton for 30 minutes at RT, and then incubated with the primary antibodies diluted in the blocking solution (PBS-0,1% Triton /10% Foetal Calf Serum (FCS)) at 4°C over-night with gentle agitation. The following day, sections were washed 3 times for 5 minutes in PBS at RT, incubated 4 hours in the dark and at RT with the appropriate secondary antibodies (and DAPI if needed) diluted in PBS-0,1% Triton, washed again 3 times for 5 minutes at RT with PBS and mounted with Vectashield (with or without DAPI, depending on experiment – Vector Laboratories H-1000-10 & H-1200-10).

All immunostainings on slide-mounted cryosections were performed during and after the end of ISH revelation protocol. Slides were incubated with primary antibodies during the appropriate step described above in the Cryostat sections and In Situ Hybridization section. After ISH signal revelation, slides were incubated 4 hours in the dark and at RT with 250µl of appropriate secondary antibodies (and DAPI, if needed) diluted in PBS-0,1% Triton, washed again 3 times for 5 minutes at RT with PBS and mounted with Aquatex.

Primary antibodies used are: chick anti-GFP (GFP-1020 – 1:2000) from Aves Labs; goat anti-Sox2 (clone Y-17 – 1:1000) from Santa Cruz; rabbit anti-pRb (Ser807/811 – 1:1000) from Cell Signaling; mouse anti c-myc tag (Clone 9E10 - 1:100) from Sigma-Aldrich; rabbit anti DsRed (Polyclonal - 1: 400) from Takara Bio; mouse anti-HuC/D (clone 16A11 – 1:50) from Life Technologies. Secondary antibodies coupled to Alexa Fluor 488, Cy3 or Alexa Fluor 649 were all obtained from Jackson laboratories and all used at a 1:500 dilutions.

EdU labelling

Proliferating progenitors in the neural tube were labelled with 5-ethynyl-2'-deoxyuridine (EdU) via *in ovo* incorporation. Before EdU injection, membranes surrounding the embryos were slightly opened using forceps. For 1h pulse experiments, 100µl of a 500 µM solution of

EdU diluted in PBS was deposited in the previously opened space. For cumulative EdU labelling, embryos were incubated with EdU for the appropriate amount of time before collection. In this context, 100µl of a 500 µM solution of EdU diluted in PBS was deposited every 6 hours in the previously opened space after initial injection. After collection, embryos were subsequently processed following the vibratome sections protocol. Revelation of EdU incorporated in progenitors was carried out on vibratome sections after the permeabilization step, using the Click-iT EdU imaging kit according to manufacturer's protocol (Invitrogen).

FlashTag preparation and injection

A 1mM stock solution of CellTrace Far Red (Life Technologies, #C34564 - (Baek et al., 2018a)) was prepared by adding 20µl of DMSO to a CellTrace Far red dye stock vial. A working solution of 100µM was subsequently prepared by diluting 1µl of stock solution in 9µl of 37°C preheated PBS, and injected directly into E3 chick neural tubes. The eggs were resealed with parafilm and embryos were incubated at 38 °C for the appropriate time until dissection.

Image Acquisition

Transverse sections of chick embryo neural tubes after ISH and/or immunofluorescence were obtained either on a confocal microscope (model SP5; Leica) using 40× and 63× (Plan Neofluar NA 1.3 oil immersion) objectives and Leica LAS software, or on an inverted microscope (Nikon TiEclipse) equipped with a Yokogawa CSU-WI spinning disk confocal head, a Borealis system (Andor Technologies) and an sCMOS Camera (Orca Flash4LT, Hamamatsu) using a 40× objective (CFI Plan APO LBDA, NA 0.45, Nikon) or a 100× oil immersion objective (APO VC, NA 1.4, Nikon) and micromanager software (Edelstein et al, 2010). For image processing, data analysis and quantifications, we used the Fiji software to adjust brightness and contrast

Image Quantifications

In the ventral motor neuron domain of the neural tube, progenitors differentiate earlier than in any other region of the NT. Thus, to reason on a more homogeneous progenitor population, we restricted all our analysis to the dorsal two thirds of the NT. All cell counting in this study were performed manually.

Status of proliferation/differentiation balance at tissue level.

HH13-14 chick embryos were electroporated with specific shRNAs (described below for each Figure) and status of the proliferation/differentiation balance was analysed one or two days after electroporation.

Unambiguous identification of cycling progenitors and postmitotic neurons is notoriously difficult in the chick spinal cord, as there are no reliable reagents that label these populations: markers of neurons, such as HuC/D of bIII-tubulin (TujI) are not detected during the first hours of neural differentiation; on the other hand, markers of progenitors usually either do not label all the phases of the cell cycle (eg. pRb), or persist transiently in newborn neurons (eg. Sox2). With these limitations in mind, we used antibodies against HuC/D to label neurons, and either a pRb antibody to identify the progenitor population. For conditions analysed using a combination of GFP, phospho-Rb and HuC/D primary antibodies, three ratios were determined. Progenitor ratio was obtained by dividing the number of shRNA transfected (GFP-positive) and pRb-positive/HuC/D-negative cells by the total number of transfected cells (GFP-positive). Neuron ratio was obtained by counting the number of shRNA transfected (GFP) HuC/D-positive cells over the total number of transfected cells (GFP positive); and Undetermined ratio was obtained by dividing the number of shRNA transfected (GFP positive) cells that were negative for both pRb and HuC/D by the total number of transfected cells (GFP positive).

Cumulative EdU incorporation in Cdkn1c and control knock-down progenitors

Chick embryos were electroporated at E2 with either Control shRNA or cCdkn1c shRNA 1 and EdU injections were performed *in ovo* starting at E3 and then every 6 hours to cover the whole cell cycle.

At each measured timepoint (1h, 4h, 7h, 10h, 12h, 14 and 17h after the first EdU injection), we quantified the number of Edu-positive electroporated progenitors (triple positive for EdU, pRb and GFP) over the total population of electroporated progenitor cells (pRb and GFP positive) (Figure 3B). Cycling progenitor graphs were then constructed by plotting the obtained average values for each timepoint. The numbers of embryos, sections and cells quantified for each timepoint in each condition is detailed below.

cCDKN1C shRNA 1 condition: A minimum of 730 cells, collected from 3 to 5 embryos were analysed for each timepoint, from 1 to 2 different experiments.

Control shRNA condition: A minimum of 689 cells, collected from 2 to 5 embryos were analysed for each timepoint, from 1 to 2 different experiments.

Quantification of progenitors in S phase at a given time point (1h EdU pulse).

Control shRNA vs single cCDKN1C shRNA 1 vs single cCCND1 shRNA vs double cCDKN1C + cCCND1 shRNAs were electroporated in HH13-14 chick embryos. One or two days after shRNAs electroporation (and a reporter of electroporation (GFP) for cCCND1 shRNA alone), we injected EdU *in ovo* one hour before collecting the embryos, then labelled transverse sections for EdU incorporation. We then quantified the proportion of progenitors in S-phase in the shRNA conditions (GFP/EdU/pRb-positive cells) over the global population of electroporated progenitors (GFP/pRb-positive). The numbers of embryos, sections and cells quantified for each timepoint in each condition is detailed below. Post-EP = post-Electroporation. For the CDKN1C shRNA 1, values at 24h post-EP were re-used from cumulative cell cycle values obtained previously.

24h post-electroporation: For each condition, a minimum of 730 cells collected from 3 to 6 embryos were analysed; 48h post-electroporation: For each condition, a minimum of 1594 cells collected from 3 to 6 embryos were analysed

G1 analysis of neural progenitors at the cell level.

We used the FlashTag (FT) technique, based on the ability of the cell-permeant dye CellTrace Far Red (Life Technologies, #C34564) to fluorescently label intracellular proteins. Previous experiments in the embryonic chick have shown that upon direct injection in the neural tube, FT dyes preferentially enter progenitor cells undergoing mitosis near the apical surface and that this incorporation only occurs during a 15-30 minutes' time window (Baek et al., 2018). Since FT fluorescence is preserved in daughter cells after mitosis, this dye offers a convenient means to synchronously label a cohort of cells dividing at the time of injection and follow their progeny.

Using a combination of FT injection and cumulative EdU incorporation allows to monitor precisely the average length of the G1 phase. Daughter cells from FT positive progenitors enter G0/G1 phase just after mitosis, and will start incorporating EdU only when entering S phase. For each cell in a FT cohort, the time window between FT injection and the beginning of EdU incorporation corresponds to the duration of the G1 phase. One day after electroporation, FT and EdU were injected simultaneously and embryos were collected at different time points after injection to identify the time at which all cells in the FT cohort have exited G1 and entered S-phase. For time points over 6 hours, an additional EdU injection was performed after 6 hours to cumulatively label the whole population of cycling cells.

We quantified the number of electroporated (GFP+) progenitors (pRb+) having incorporated EdU and FT (GFP/pRb/EdU/FT quadruple positive) relative to the number of FT electroporated progenitors (GFP/pRb/FT triple positive). At each time point, the percentage of quadruple positive cells represents the proportion of progenitors having completed their G1 phase. This percentage reaches a plateau when all the progenitors in the FT cohort have entered S-phase. Therefore, an experimental FT cohort that reaches the plateau faster than the control FT cohort has a shorter G1 phase duration.

Clonal analysis of sister cell identities and mode of division

We first determined the time point after mitosis at which pRb becomes a reliable progenitor marker by monitoring the time window after which all progenitors in a synchronized cohort of cells undergoing mitosis reach the restriction point/late G1 stage, as determined by pRb immunoreactivity. Using FT to label a cohort of pairs of sister cells that perform their division synchronously at E3, we counted the proportion of pairs in the cohort that contained 0, 1 or 2 cells positive for pRb at different time points after FT injection. The distribution between these three categories should reach a plateau when all the progenitors in the cohort have passed the restriction point and have become positive for pRb. At E3, this plateau was reached between 4h30 and 6 hours after injection, and the distribution of pRb immunoreactivity within pairs of FT-positive sister cells was stable at later time points, indicating that from 6 hours after FT injection, the proportions of FT pairs with 0, 1, or 2 pRb-positive cells respectively correspond to the proportions of NN, PN and PP pairs in the cohort. We therefore choose to perform clonal analysis in embryos harvested 6 hours after FT injection.

Chick embryos were electroporated at E2 with the relevant shRNAs. One day later FlashTag was injected in the neural tubes in order to follow the progeny of isochronic dividing neural progenitors. Cell identity of transfected GFP positive cells was determined as follows: cells positive for pRb and FlashTag were classified as progenitors and cells positive for FlashTag and negative for pRb as neurons. In addition, a similar intensity of both the GFP and FT signals within pairs of cells, as well as their proximity within the tissue were used as criteria to further ascertain sisterhood. Using these criteria to identify pairs of sister cells, the mode of division used by their mother cell was determined as follows: symmetric if the two daughter cells were attributed the progenitor identity (PP); asymmetric if one of the daughters was a progenitor and the other daughter a neuron (PN); and terminal if the two daughter cells had a neuronal identity (NN).

Statistical analyses

The number of embryos and analysed cells or sections are indicated above. All data processing and statistical analyses were performed using Excel and GraphPad Prism software and are indicated in Legends to Figures.

Contact for Reagent and Resource Sharing

As Lead Contact, Xavier Morin (Institut de Biologie de l'Ecole Normale Supérieure) is responsible for all reagent and resource requests. Please contact Xavier Morin at

xavier.morin@bio.ens.psl.eu with requests and enquiries.

Key Resources Table – STAR METHODS

REAGENT OR RESSOURCE	SOURCE	IDENTIFIER
Antibodies		
Chick anti-GFP	Aves Labs	Cat#GFP-1020 RRID : AB_10000240

Goat anti-Sox2 (clone Y-17)	Santa Cruz	Cat#Sc-17320 RRID : AB_2286684
Rabbit anti-pRb (Ser807/811)	Cell Signaling	Cat# 8516S RRID : AB_331472
Mouse anti-HuC/D (clone 16A11)	ThermoFisher Scientific	Cat#A-21271 RRID : AB_221448
Mouse anti c-myc tag	Sigma-Aldrich	Cat# MABE5282 RRID : N/A
Rabbit anti-DsRed	Takara Bio	Cat#632496 RRID : N/A
Experimental Models : Organisms/Strains		
Chick fertilized eggs	EARL Morizeau	JA57
Recombinant DNA		
PTol2-H2B-EGP	Peyre et al, 2011	N/A
PTol2-H2B-EGP Luciferase	Peyre et al, 2011	N/A
pGFP-cCDKN1C shRNA1	This paper	N/A
pGFP-cCDKN1C shRNA2	This paper	N/A
pGFP-cCDKN1C shRNA3	This paper	N/A
pGFP-cCDKN1C shRNA4	This paper	N/A
pGFP-cCDKN1C shRNA5	This paper	N/A
pGFP-cCDKN1C shRNA6	This paper	N/A
cCCND1 siRNA	(Lukaszewicz and Anderson, 2011b)	N/A
pCAGGS	Niwa et al, 1991	N/A
pCX-H2B-EGFP	Gift from K. Hadjantonakis	N/A
Oligonucleotides		
General oligonucleotide: First hairpin primer 5’ 5’-ggcggggctagctggagaagatgccttccggagaggtgctgctgagcg-3’	Eurofins Genomics	N/A
General oligonucleotide: First hairpin primer 3’ 5’-gggtggacgcgtaagaggggaagaaagcttctaaccccgctattcaccaccactaggca-3’	Eurofins Genomics	N/A
Target forward sequence cCDKN1C shRNA1 5’-gagaggtgctgctgagcgaggcaccgtgcccgcgttctatagtgagccacagatgta-3’	Eurofins Genomics	N/A
Target reverse sequence cCDKN1C shRNA1 5’-attcaccaccactaggcacggcaccgtgcccgcgttctatacatctgtggcttcact-3’	Eurofins Genomics	N/A
Target forward sequence cCDKN1C shRNA2 5’-gagaggtgctgctgagcgtacgacccgcatcacagattttagtgaaccacagatgta-3’	Eurofins Genomics	N/A
Target reverse sequence cCDKN1C shRNA2 5’-attcaccaccactaggcacacgacccgcatcacagattttacatctgtggcttcact-3’	Eurofins Genomics	N/A
Target forward sequence cCDKN1C shRNA3 5’-gagaggtgctgctgagcgggcgccgtctgcaggagcttatagtgaaccacagatgta-3’	Eurofins Genomics	N/A

Target reverse sequence cCDKN1C shRNA3 5’-attcaccaccactaggcaagcgccgtctgcaggagcttatacatctgtggcttcact-3’	Eurofins Genomics	N/A
Target forward sequence cCDKN1C shRNA4 5’-gagaggtgctgctgagcgtgagccgggagaaccgcgccgtagtgaagccacagatgta-3’	Eurofins Genomics	N/A
Target reverse sequence cCDKN1C shRNA4 5’-attcaccaccactaggcatgagccgggagaaccgcgccgtacatctgtggcttcact-3’	Eurofins Genomics	N/A
Target forward sequence cCDKN1C shRNA5 5’-gagaggtgctgctgagcgcgacccgcatcacagatttcttagtgaagccacagatgta-3’	Eurofins Genomics	N/A
Target reverse sequence cCDKN1C shRNA5 5’-attcaccaccactaggcacgacccgcatcacagatttcttacatctgtggcttcact-3’	Eurofins Genomics	N/A
Target forward sequence cCDKN1C shRNA6 5’-gagaggtgctgctgagcgctcaataaacaaaacaaaaaatagtgaagccacagatgta-3’	Eurofins Genomics	N/A
Target reverse sequence cCDKN1C shRNA6 5’-attcaccaccactaggcactcaataaacaaaacaaaaaatacatctgtggcttcact-3’	Eurofins Genomics	N/A
Target forward sequence cCDKN1C gRNA1 5’-CACCGCTGAGCACACCCCCCGCAAG -3’	Eurofins Genomics	N/A
Target reverse sequence cCDKN1C gRNA1 5’-AAAGCTTGCGGGGGGTGTGCTCAGC -3’	Eurofins Genomics	N/A
Target forward sequence cCDKN1C gRNA1 5’-CACCGCGGCTCCGCTGAGCCAGGTG -3’	Eurofins Genomics	N/A
Target reverse sequence cCDKN1C gRNA1 5’-AAAGCACCTGGCTCAGCGGAGCCGC-3’	Eurofins Genomics	N/A
Target forward sequence cCDKN1C gRNA1 5’-CACCGAGCTCCTCACCTGGCTCAG -3’	Eurofins Genomics	N/A
Target reverse sequence cCDKN1C gRNA1 5’-AAAGCTGAGCCAGGTGAGGAGCTC-3’	Eurofins Genomics	N/A
Target forward sequence Pax7 gRNA1 5’-CACCGCCTGTCTCTACTGGTAGGAG-3’	Eurofins Genomics	N/A
Target reverse sequence Pax7 gRNA1 5’-AAAGCTCCTACCAGTAGAGACAGGC -3’	Eurofins Genomics	N/A
Softwares		
ImageJ	(Schneider et al., 2012)	http://imagej.net/Welcome RRID: SCR_003070
Graphpad Prism	Graphpad	http://www.graphpad.com/ RRID: SCR_002798
Microsoft Excel	Microsoft	RRID: SCR_016137
MicroManager	(Edelstein et al., 2010)	https://micro-manager.org/ RRID: SCR_000415
Affinity Publisher	Affinity	N/A

ACKNOWLEDGEMENTS

We thank our colleague Samuel Tozer for discussions and critical reading of the manuscript. We thank Fabienne Pituello and Matthew Towers for plasmids. We thank Benjamin Bunel for the original drafting of the figures. This work was supported by grants from the Fondation pour la Recherche Medicale (FRM EQU202003010547), the Labex MEMO LIFE, the Fondation Cino del Duca to XM, the Institut Universitaire de France to MTC and a joint grant from the Agence Nationale pour la Recherche (SYMASYM ANR-18-CE16-0021-01) to MTC and XM. B. Mida was supported by doctoral grants from the French Ministry of Higher Education and Research (MESR) and the Labex MEMO LIFE. This work has received support under the program « Investissements d'Avenir » launched by the French Government and implemented by the ANR, with the reference ANR-10-LABX-54 MEMO LIFE. The GenomiqueENS core facility was supported by the France Génomique national infrastructure, funded as part of the "Investissements d'Avenir" program managed by the Agence Nationale de la Recherche (contract ANR-10-INBS-09). The authors declare no competing financial interests.

AUTHOR CONTRIBUTIONS

Conceptualization – E.F., X.M.

Data curation – N.L.

Formal analysis – N.L, B.M.

Funding acquisition – M.T.-C., X.M.

Investigation – B.M., F.C., R.G., K.B.

Methodology – N.L., M.T.-C., E.F., X.M.

Project administration – M.T.-C., E.F., X.M.

Software – N.L.

Supervision – M.T.-C., E.F., X.M.

Validation – E.F., X.M.

Visualization – B.M., N.L., E.F., X.M.

Writing – original draft – E.F., X.M.

Writing – review & editing – N.L., M.T.-C., E.F., X.M.

Competing interests : "Authors declare that they have no competing interests."

REFERENCES

Albert, M., Kalebic, N., Florio, M., Lakshmanaperumal, N., Haffner, C., Brandl, H., Henry, I., Huttner, W.B., 2017. Epigenome profiling and editing of neocortical progenitor cells during development. EMBO J. 36, 2642–2658. https://doi.org/10.15252/embj.201796764

Aprea, J., Prenninger, S., Dori, M., Ghosh, T., Monasor, L.S., Wessendorf, E., Zocher, S., Massalini, S., Alexopoulou, D., Lesche, M., Dahl, A., Groszer, M., Hiller, M., Calegari, F., 2013. Transcriptome sequencing during mouse brain development identifies long non-coding RNAs functionally involved in neurogenic commitment. EMBO J. 32, 3145–3160. https://doi.org/10.1038/emboj.2013.245

Arai, Y., Pulvers, J.N., Haffner, C., Schilling, B., Nüsslein, I., Calegari, F., Huttner, W.B., 2011. Neural stem and progenitor cells shorten S-phase on commitment to neuron production. Nat. Commun. 2, 154. https://doi.org/10.1038/ncomms1155

Baek, C., Freem, L., Goïame, R., Sang, H., Morin, X., Tozer, S., 2018a. Mib1 prevents Notch Cis-inhibition to defer differentiation and preserve neuroepithelial integrity during neural delamination. PLoS Biol. 16, e2004162. https://doi.org/10.1371/journal.pbio.2004162

Bonnet, F., Molina, A., Roussat, M., Azais, M., Bel-Vialar, S., Gautrais, J., Pituello, F., Agius, E., 2018. Neurogenic decisions require a cell cycle independent function of the CDC25B phosphatase. Elife 3;7:e32937. https://doi.org/10.7554/eLife.32937.

Calegari, F., Haubensak, W., Haffner, C., Huttner, W.B., 2005. Selective lengthening of the cell cycle in the neurogenic subpopulation of neural progenitor cells during mouse brain development. J Neurosci 13;25(28):6533–8. https://doi.org/10.1523/JNEUROSCI.0778-05.2005.

Calegari, F., Huttner, W.B., 2003. An inhibition of cyclin-dependent kinases that lengthens, but does not arrest, neuroepithelial cell cycle induces premature neurogenesis. J Cell Sci 15;116(Pt 24):4947-55. https://doi.org/10.1242/jcs.00825.

Cong, L., Ran, F.A., Cox, D., Lin, S., Barretto, R., Habib, N., Hsu, P.D., Wu, X., Jiang, W., Marraffini, L.A., Zhang, F., 2013. Multiplex genome engineering using CRISPR/Cas systems. Science 339, 819–823. https://doi.org/10.1126/science.1231143

Creff, J., Besson, A., 2020. Functional Versatility of the CDK Inhibitor p57Kip2. Front. Cell Dev. Biol. 8, 584590. https://doi.org/10.3389/fcell.2020.584590

Darnat, P., Burg, A., Sallé, J., Lacoste, J., Louvet-Vallée, S., Gho, M., Audibert, A., 2022. Cortical Cyclin A controls spindle orientation during asymmetric cell divisions in Drosophila. Nat. Commun. 13, 2723. https://doi.org/10.1038/s41467-022-30182-1

Das, R.M., Van Hateren, N.J., Howell, G.R., Farrell, E.R., Bangs, F.K., Porteous, V.C., Manning, E.M., McGrew, M.J., Ohyama, K., Sacco, M.A., Halley, P.A., Sang, H.M., Storey, K.G., Placzek, M., Tickle, C., Nair, V.K., Wilson, S.A., 2006. A robust system for RNA interference in the chicken using a modified microRNA operon. Dev. Biol. 294, 554–563. https://doi.org/10.1016/j.ydbio.2006.02.020

Delile, J., Rayon, T., Melchionda, M., Edwards, A., Briscoe, J., Sagner, A., 2019. Single cell transcriptomics reveals spatial and temporal dynamics of gene expression in the developing mouse spinal cord. Development dev.173807. https://doi.org/10.1242/dev.173807

Edelstein, A., Amodaj, N., Hoover, K., Vale, R., Stuurman, N., 2010. Computer control of microscopes using µManager. Curr. Protoc. Mol. Biol. Chapter 14, Unit14.20. https://doi.org/10.1002/0471142727.mb1420s92

Fior, R., Henrique, D., 2005. A novel hes5/hes6 circuitry of negative regulation controls Notch activity during neurogenesis. Dev. Biol. 281, 318–333. https://doi.org/10.1016/j.ydbio.2005.03.017

FUJITA, S., 1962. Kinetics of cellular proliferation. Exp Cell Res.

Gandhi, S., Piacentino, M.L., Vieceli, F.M., Bronner, M.E., 2017. Optimization of CRISPR/Cas9 genome editing for loss-of-function in the early chick embryo. Dev. Biol. 432, 86–97. https://doi.org/10.1016/j.ydbio.2017.08.036

Gao, P., Postiglione, M.P., Krieger, T.G., Hernandez, L., Wang, C., Han, Z., Streicher, C., Papusheva, E., Insolera, R., Chugh, K., Kodish, O., Huang, K., Simons, B.D., Luo, L., Hippenmeyer, S., Shi, S.-H., 2014. Deterministic Progenitor Behavior and Unitary Production of Neurons in the Neocortex. Cell 159, 775–788. https://doi.org/10.1016/j.cell.2014.10.027

Georgia, S., Soliz, R., Li, M., Zhang, P., Bhushan, A., 2006. p57 and Hes1 coordinate cell cycle exit with self-renewal of pancreatic progenitors. Dev. Biol. 298, 22–31. https://doi.org/10.1016/j.ydbio.2006.05.036

Gui, H., Li, S., Matise, M.P., 2007. A cell-autonomous requirement for Cip/Kip Cyclin-kinase inhibitors in regulating the timing of neuronal cell cycle exit but not differentiation in the developing spinal cord. Dev. Biol. 301, 14–26. https://doi.org/10.1016/j.ydbio.2006.10.035

Hamburger, V., Hamilton, H.L., 1992. A series of normal stages in the development of the chick embryo. 1951. Dev. Dyn. Off. Publ. Am. Assoc. Anat. 195, 231–272. https://doi.org/10.1002/aja.1001950404

Hämmerle, B., Vera-Samper, E., Speicher, S., Arencibia, R., Martínez, S., Tejedor, F.J., 2002. Mnb/Dyrk1A Is Transiently Expressed and Asymmetrically Segregated in Neural Progenitor Cells at the Transition to Neurogenic Divisions. Dev. Biol. 246, 259–273. https://doi.org/10.1006/dbio.2002.0675

Haubensak, W., Attardo, A., Denk, W., Huttner, W.B., 2004a. Neurons arise in the basal neuroepithelium of the early mammalian telencephalon: A major site of neurogenesis. Proc. Natl. Acad. Sci. 101, 3196–3201. https://doi.org/10.1073/pnas.0308600100

Iacopetti, P., Michelini, M., Stuckmann, I., Oback, B., Aaku-Saraste, E., Huttner, W.B., 1999. Expression of the antiproliferative gene TIS21 at the onset of neurogenesis identifies single neuroepithelial cells that switch from proliferative to neuron-generating division. Proc Natl Acad Sci U A 13;96(8):4639-44. https://doi.org/10.1073/pnas.96.8.4639.

Kicheva, A., Bollenbach, T., Ribeiro, A., Valle, H.P., Lovell-Badge, R., Episkopou, V., Briscoe, J., 2014. Coordination of progenitor specification and growth in mouse and chick spinal cord. Science 345, 1254927. https://doi.org/10.1126/science.1254927

Lacomme, M., Liaubet, L., Pituello, F., Bel-Vialar, S., 2012. NEUROG2 Drives Cell Cycle Exit of Neuronal Precursors by Specifically Repressing a Subset of Cyclins Acting at the G1 and S Phases of the Cell Cycle. Mol. Cell. Biol. 32, 2596–2607. https://doi.org/10.1128/MCB.06745-11

Lange, C., Huttner, W.B., Calegari, F., 2009. Cdk4/cyclinD1 overexpression in neural stem cells shortens G1, delays neurogenesis, and promotes the generation and expansion of basal progenitors. Cell Stem Cell 4;5(3):320-31. https://doi.org/10.1016/j.stem.2009.05.026.

Lee, M.H., Reynisdóttir, I., Massagué, J., 1995. Cloning of p57KIP2, a cyclin-dependent kinase inhibitor with unique domain structure and tissue distribution. Genes Dev 15;9(6):639-49. https://doi.org/10.1101/gad.9.6.639.

Lehmann, N., Perrin, S., Wallon, C., Bauquet, X., Deshaies, V., Firmo, C., Du, R., Berthelier, C., Hernandez, C., Michaud, C., Thieffry, D., Crom, S.L., Thomas-Chollier, M., Jourdren, L., 2021. Eoulsan 2: an efficient workflow manager for reproducible bulk, long-read and single-cell transcriptomics analyses. https://doi.org/10.1101/2021.10.13.464219

Lobjois, V., Benazeraf, B., Bertrand, N., Medevielle, F., Pituello, F., 2004. Specific regulation of cyclins D1 and D2 by FGF and Shh signaling coordinates cell cycle progression, patterning, and differentiation during early steps of spinal cord development. Dev. Biol. 273, 195–209. https://doi.org/10.1016/j.ydbio.2004.05.031

Lukaszewicz, A.I., Anderson, D.J., 2011a. Cyclin D1 promotes neurogenesis in the developing spinal cord in a cell cycle-independent manner. Proc. Natl. Acad. Sci. U. S. A. 108, 11632–11637. https://doi.org/10.1073/pnas.1106230108

Mairet-Coello, G., Tury, A., Van Buskirk, E., Robinson, K., Genestine, M., DiCicco-Bloom, E., 2012a. p57KIP2 regulates radial glia and intermediate precursor cell cycle dynamics and lower layer neurogenesis in developing cerebral cortex. Development 139, 475–487. https://doi.org/10.1242/dev.067314

Matsuoka, S., Edwards, M.C., Bai, C., Parker, S., Zhang, P., Baldini, A., Harper, J.W., Elledge, S.J., 1995. p57KIP2, a structurally distinct member of the p21CIP1 Cdk inhibitor family, is a candidate tumor suppressor gene. Genes Dev. 9, 650–662. https://doi.org/10.1101/gad.9.6.650

Nguyen, L., Besson, A., Heng, J.I.-T., Schuurmans, C., Teboul, L., Parras, C., Philpott, A., Roberts, J.M., Guillemot, F., 2006. p27 ^{kip1} independently promotes neuronal differentiation and migration in the cerebral cortex. Genes Dev. 20, 1511–1524. https://doi.org/10.1101/gad.377106

Noctor, S.C., Flint, A.C., Weissman, T.A., Dammerman, R.S., Kriegstein, A.R., 2001. Neurons derived from radial glial cells establish radial units in neocortex. Nature 409, 714–720. https://doi.org/10.1038/35055553

Noctor, S.C., Martínez-Cerdeño, V., Ivic, L., Kriegstein, A.R., 2004. Cortical neurons arise in symmetric and asymmetric division zones and migrate through specific phases. Nat. Neurosci. 7, 136–144. https://doi.org/10.1038/nn1172

Nowakowski, R.S., Lewin, S.B., Miller, M.W., 1989. Bromodeoxyuridine immunohistochemical determination of the lengths of the cell cycle and the DNA-synthetic phase for an anatomically defined population. J. Neurocytol. 18, 311–318. https://doi.org/10.1007/BF01190834

Peyre, E., Jaouen, F., Saadaoui, M., Haren, L., Merdes, A., Durbec, P., Morin, X., 2011. A lateral belt of cortical LGN and NuMA guides mitotic spindle movements and planar division in neuroepithelial cells. J. Cell Biol. 193, 141–154. https://doi.org/10.1083/jcb.201101039

Peyre, E., Morin, X., 2012. An oblique view on the role of spindle orientation in vertebrate neurogenesis. Dev. Growth Differ. 54, 287–305. https://doi.org/10.1111/j.1440-169X.2012.01350.x

Pickering, J., Chinnaiya, K., Towers, M., 2019. An autoregulatory cell cycle timer integrates growth and specification in chick wing digit development. eLife 8, e47625. https://doi.org/10.7554/eLife.47625

Pietro, F. di, Valon, L., Li, Y., Goïame, R., Genovesio, A., Morin, X., 2017. An RNAi Screen in a Novel Model of Oriented Divisions Identifies the Actin-Capping Protein Z β as an Essential Regulator of Spindle Orientation. Curr. Biol. 27, 2452-2464.e8. https://doi.org/10.1016/j.cub.2017.06.055

Pilaz, L.-J., Patti, D., Marcy, G., Ollier, E., Pfister, S., Douglas, R.J., Betizeau, M., Gautier, E., Cortay, V., Doerflinger, N., Kennedy, H., Dehay, C., 2009. Forced G1-phase reduction alters mode of division, neuron number, and laminar phenotype in the cerebral cortex. Proc. Natl. Acad. Sci. 106, 21924–21929. https://doi.org/10.1073/pnas.0909894106

Prjibelski, A.D., Mikheenko, A., Joglekar, A., Smetanin, A., Jarroux, J., Lapidus, A.L., Tilgner, H.U., 2023. Accurate isoform discovery with IsoQuant using long reads. Nat. Biotechnol. 41, 915–918. https://doi.org/10.1038/s41587-022-01565-y

Saade, M., Gonzalez-Gobartt, E., Escalona, R., Usieto, S., Martí, E., 2017. Shh-mediated centrosomal recruitment of PKA promotes symmetric proliferative neuroepithelial cell division. Nat. Cell Biol. 19, 493–503. https://doi.org/10.1038/ncb3512

Saade, M., Gutiérrez-Vallejo, I., Le Dréau, G., Rabadán, M.A., Miguez, D.G., Buceta, J., Martí, E., 2013. Sonic hedgehog signaling switches the mode of division in the developing nervous system. Cell Rep 15;4(3):492-503. https://doi.org/10.1016/j.celrep.2013.06.038.

Schneider, C.A., Rasband, W.S., Eliceiri, K.W., 2012. NIH Image to ImageJ: 25 years of image analysis. Nat. Methods 9, 671–675. https://doi.org/10.1038/nmeth.2089

Smith, J.L., Schoenwolf, G.C., 1987. Cell cycle and neuroepithelial cell shape during bending of the chick neural plate. Anat Rec Jun;218(2):196-206. https://doi.org/10.1002/ar.1092180215.

Takahashi, T., Nowakowski, R.S., VS, C., Jr, 1995. The cell cycle of the pseudostratified ventricular epithelium of the embryonic murine cerebral wall. J Neurosci. https://doi.org/10.1523/JNEUROSCI.15-09-06046.1995.

Taverna, E., Götz, M., Huttner, W.B., 2014. The cell biology of neurogenesis: toward an understanding of the development and evolution of the neocortex. Annu. Rev. Cell Dev. Biol. 30, 465–502. https://doi.org/10.1146/annurev-cellbio-101011-155801

Telley, L., Govindan, S., Prados, J., Stevant, I., Nef, S., Dermitzakis, E., Dayer, A., Jabaudon, D., 2016. Sequential transcriptional waves direct the differentiation of newborn neurons in the mouse neocortex. Science 351, 1443–1446. https://doi.org/10.1126/science.aad8361

Tio, M., Udolph, G., Yang, X., Chia, W., 2001. cdc2 links the Drosophila cell cycle and asymmetric division machineries. Nature 409, 1063–1067. https://doi.org/10.1038/35059124

Tozer, S., Baek, C., Fischer, E., Goiame, R., Morin, X., 2017. Differential Routing of Mindbomb1 via Centriolar Satellites Regulates Asymmetric Divisions of Neural Progenitors. Neuron 93, 542-551.e4. https://doi.org/10.1016/j.neuron.2016.12.042

Tsunekawa, Y., Britto, J.M., Takahashi, M., Polleux, F., Tan, S.-S., Osumi, N., 2012. Cyclin D2 in the basal process of neural progenitors is linked to non-equivalent cell fates: Cyclin D2 inheritance is associated with asymmetric cell fate. EMBO J. 31, 1879–1892. https://doi.org/10.1038/emboj.2012.43

Tury, A., Mairet-Coello, G., DiCicco-Bloom, E., 2011. The Cyclin-Dependent Kinase Inhibitor p57Kip2 Regulates Cell Cycle Exit, Differentiation, and Migration of Embryonic Cerebral

Cortical Precursors. Cereb. Cortex 21, 1840–1856. https://doi.org/10.1093/cercor/bhq254

Welker, J., Wierson, W., Almeida, M., Mann, C., Torrie, M., Ming, Z., Ekker, S., Clark, K., Dobbs, D., Essner, J., McGrail, M., 2021. GeneWeld: Efficient Targeted Integration Directed by Short Homology in Zebrafish. BIO-Protoc. 11. https://doi.org/10.21769/BioProtoc.4100

Zhang, X., Chen, M.H., Wu, X., Kodani, A., Fan, J., Doan, R., Ozawa, M., Ma, J., Yoshida, N., Reiter, J.F., Black, D.L., Kharchenko, P.V., Sharp, P.A., Walsh, C.A., 2016. Cell-Type-Specific Alternative Splicing Governs Cell Fate in the Developing Cerebral Cortex. Cell 166, 1147-1162.e15. https://doi.org/10.1016/j.cell.2016.07.025

FIGURES & LEGENDS

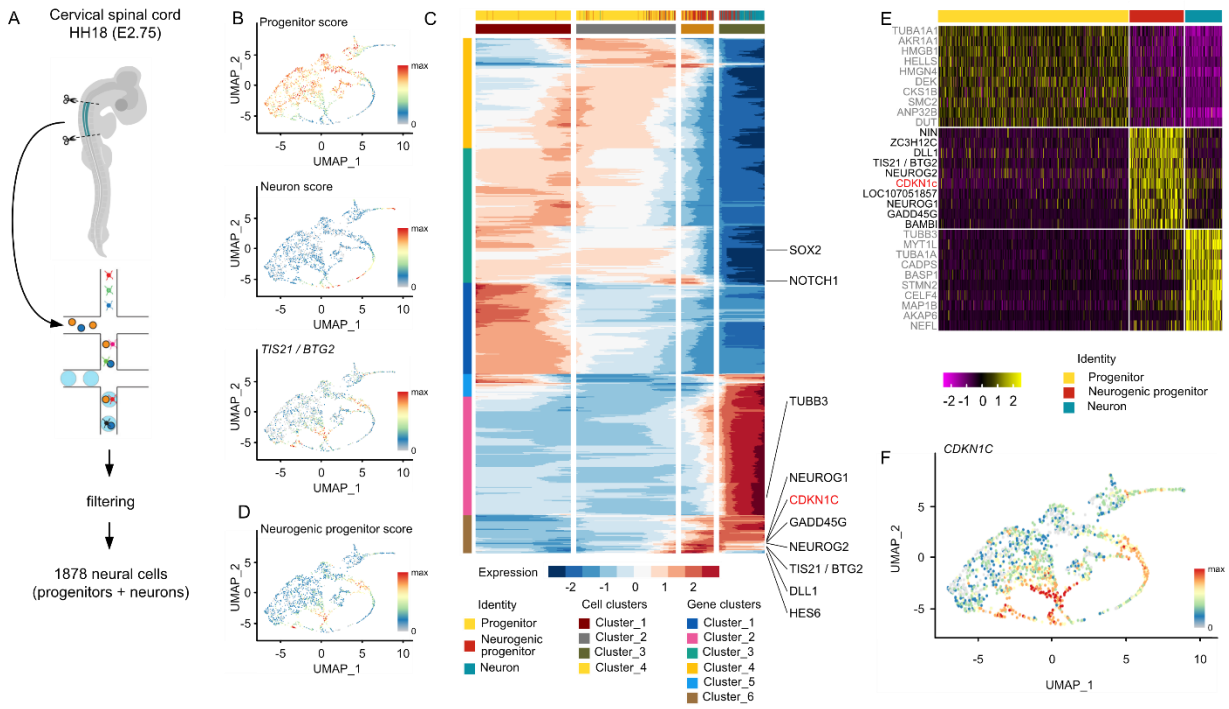

Figure 1 : scRNAseq data analyses from embryonic neural tube led to the identification of CDKN1C as a potential regulator of the transition of modes of division.

A. Scheme of the dissection and protocol for scRNA seq generation from chick cervical spinal cord at E2.75.

B. Visualization of progenitor and neuron scores and of Tis21 expression on the UMAP representation of 1878 chick cervical spinal cord neural cells.

C. Visual representation of the pseudotime analysis of the chick scRNAseq dataset. The heatmap shows the expression 6 clusters of genes with similar pattern are represented on the vertical axis. 4 cell clusters are identified on the horizontal (pseudotemporal) axis. A subset of genes used to define Progenitor, Neuron, and Neurogenic progenitor scores are indicated on the right side of the heatmap, illustrating that the 3 signatures relate to different gene clusters. A top horizontal row indicates the cell subtype assigned to each cell along the temporal axis. The blue/red color gradient represent the value of the Z-scores.

D. Visualization of neurogenic progenitor score on the UMAP representation of 1878 chick cervical spinal cord neural cells.

E. Heatmap of the 10 most differentially expressed genes between progenitor, neuron and neurogenic progenitor cell subtypes.

F. Visualization of CDKN1c expression on the UMAP representation of 1878 chick cervical spinal cord neural cells.

Mida et al., Figure 2

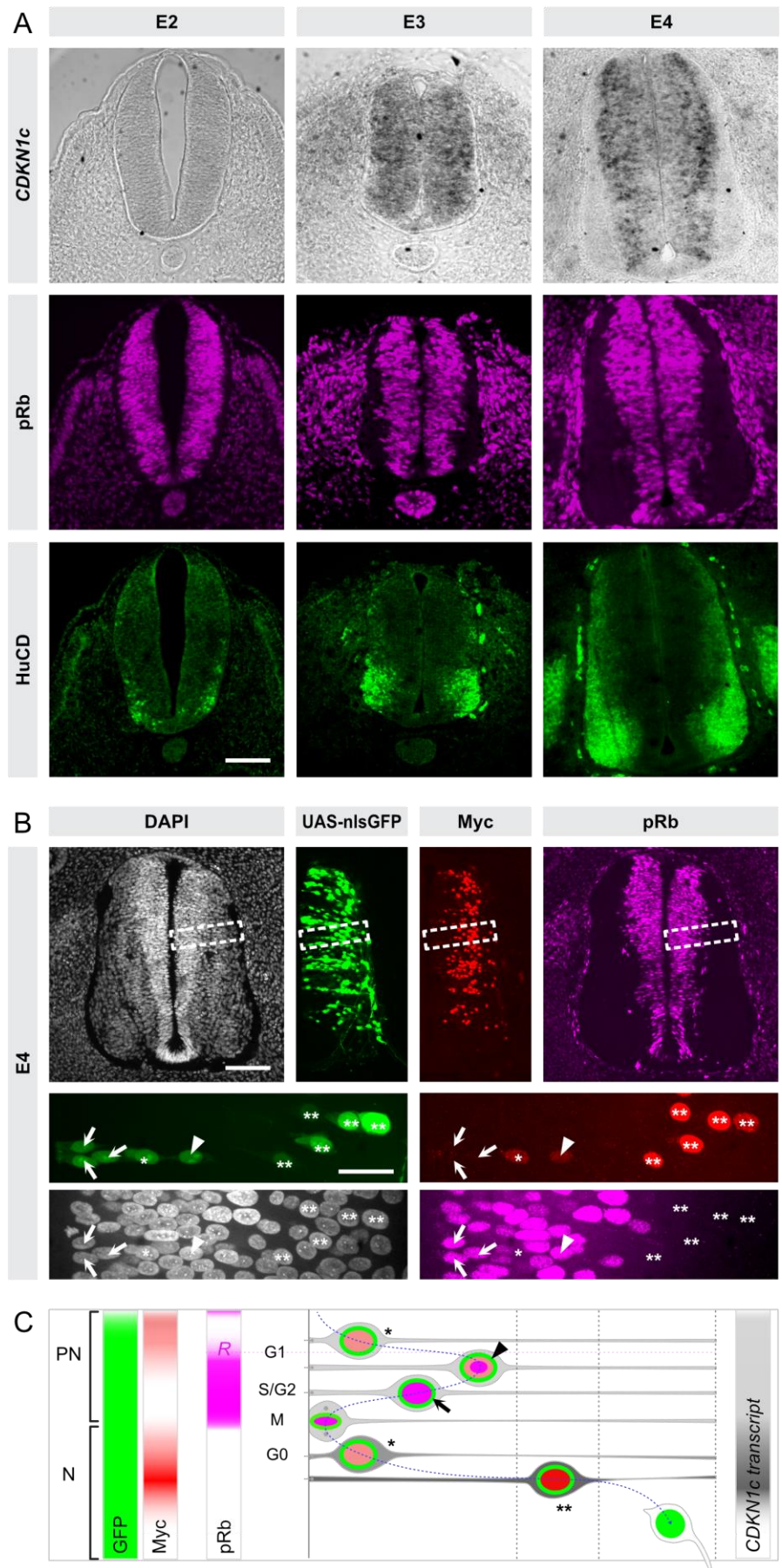

Figure 2 : Downregulation of CDKN1C impairs neurogenesis while favoring proliferation.

A mRNA expression of Cdkn1c increases during neurogenesis in chick embryonic neural tube. In situ hybridization of Cdkn1c (top row) and immunostainings for pRb (middle row, magenta) and HuCD (bottom row, green) on cryosections of thoracic region of chick embryo at sequential days during development (from left to right: E2, E3, and E4 respectively). For each stage, multichannel light and confocal fluorescence imaging are from a single section. Scale bars: 50µm.

B CDKN1c protein is detected at low level in cycling progenitors. Somatic knock-in of a Myc-tagged fused to the C-terminus of CDKN1c allows the visualization of CDKN1c protein (Myc, Red) on E4 transverse vibratome sections. Inclusion of a Gal4-VP16 transcription factor in the KI construct (see Supplementary Figure 1) identifies all the cells which express or have previously expressed but have degraded and/or stopped expressing CDKN1c via the UAS-nls-GFP reporter (green). Counter staining with a phosphor-Rb antibody (pRb, magenta) reveals cycling progenitors from late G1 to M-phase. The bottom part of the panel shows a close-up of the region highlighted by a dashed rectangle in the top panels. The key to the meaning of asterisks, arrows and arrowheads pointing to cells with different combinations of the markers is illustrated in the scheme in panel C. See main text for details. Scale bars: 50µm and 10µm in close ups.

C Scheme summarizing the dynamic expression levels of CDKN1c transcript and protein in cycling progenitors and newborn neurons, as deduced from scRNAseq, in situ hybridization and somatic KI experiments. In a subset of neurogenic progenitors (PN), the CDKN1c transcript is expressed at low levels (light gray), before it peaks transiently in newborn neurons (N, dark gray) and fades of in more mature neurons (N, white). CDKN1c protein, visualized with the Myc signal (red) is present at low levels in early G1 in neurogenic progenitors (light red nuclear signal, black asterisk) and shortly overlaps after the restriction point (R) with pRb staining (black arrowhead, light red and magenta nuclear signals). The Myc signal disappears in S/G2 (black arrow) and M phases, during which pRb is still detected (magenta nuclear signal). In newborn neurons, the CDKN1c/Myc signal is initially detected at low level (light red) and later peaks at its maximal intensity (double asterisks, dark red nucleus) during the early phases of differentiation, before fading out in mature neurons. pRb is absent in the neuronal population. The GFP signal (green) expressed from the UAS reporter is detected throughout this temporal sequence. See main text for details.

Mida et al., Figure 3

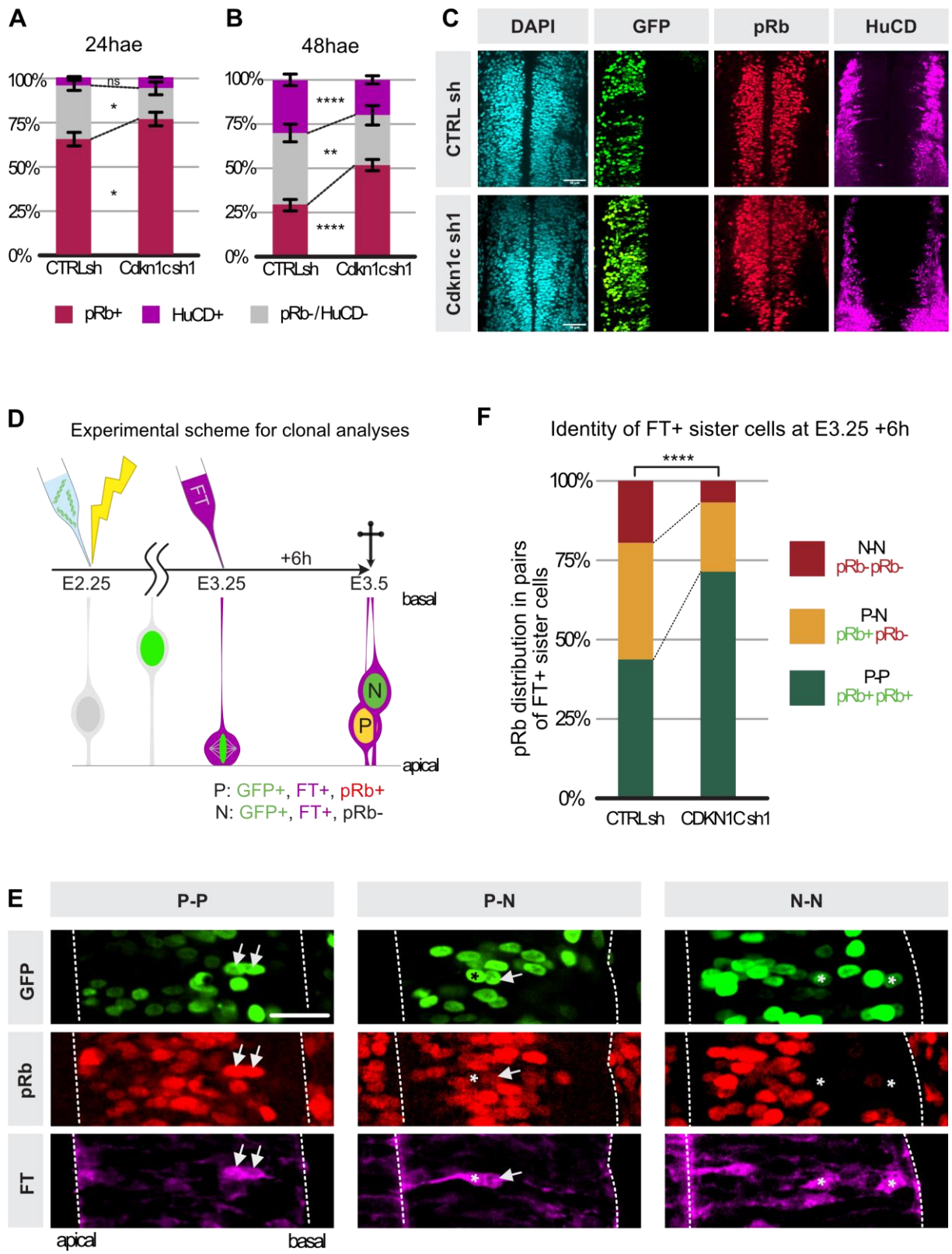

Figure 3 : Downregulation of CDKN1C delays the neurogenic transition in the spinal cord. / CDKN1C KD favors proliferative symmetric modes of division.

A Distribution of the pRb positive progenitors (dark red), HuCD positive neurons (violet) and undefined cells (double pRb/HuCD negative, gray) in shRNA or control conditions at E3 24 hours after electroporation (hae). The undefined population corresponds contains both progenitors before the restriction point (and therefore negative for pRb) and immature neurons that do not yet express HuCD. ns, $p > 0.05$; *, $p < 0.05$, (Student's unpaired t test).

B Distribution of the pRb positive progenitors (dark red), HuC/D positive neurons (violet) and undefined cells (double pRb/HuCD negative, gray) in shRNA or control conditions at E4 48 hours after electroporation (hae). ns, $p > 0.05$; **, $p < 0.01$, ***, $p < 0.001$ (Student's unpaired t test).

C: Transverse sections of the chick neural tube (thoracic level) at E4 (HH st22) stained with HuCD antibody (magenta) to label neurons and pRb (red) to label progenitors in shRNA or control conditions. Scale bar: 50µm.

D Principle of the paired-cell analysis. Embryos are co-electroporated at HH13-14 (top left, yellow thunder) with shRNA or control plasmids also expressing a H2B-EGFP reporter. Embryos are injected with the FlashTag dye 24 hours after electroporation to label a synchronous cohort of mitotic progenitors, and collected six hours later. Anti-pRb and anti-GFP Immunofluorescence on thoracic vibratome sections determines the progenitor (pRb+) or prospective neuron (pRb-) status of FlashTag-positive electroporated sister cells.

E Representative two cell clone examples in transverse neural tube sections. From left to right panels: P-P, P-N and N-N pairs. Arrows show pRb-positive (red) progenitors and asterisks show pRb-negative neurons in FlashTag-positive (magenta) pairs of GFP-positive (green) sister cells. Scale bars: 25µm

F Diagram indicating the percentage of P-P, P-N, and N-N clones for control and shRNA transfected embryos. P-P, P-N, and N-N stand for divisions producing two progenitors, one progenitor and one neuron, or two neurons, respectively. The distribution of P-P, P-N and N-N clones between control and shRNA was compared using a Chi-2 test, ****$p < 0.005$.

Mida et al, Figure 4

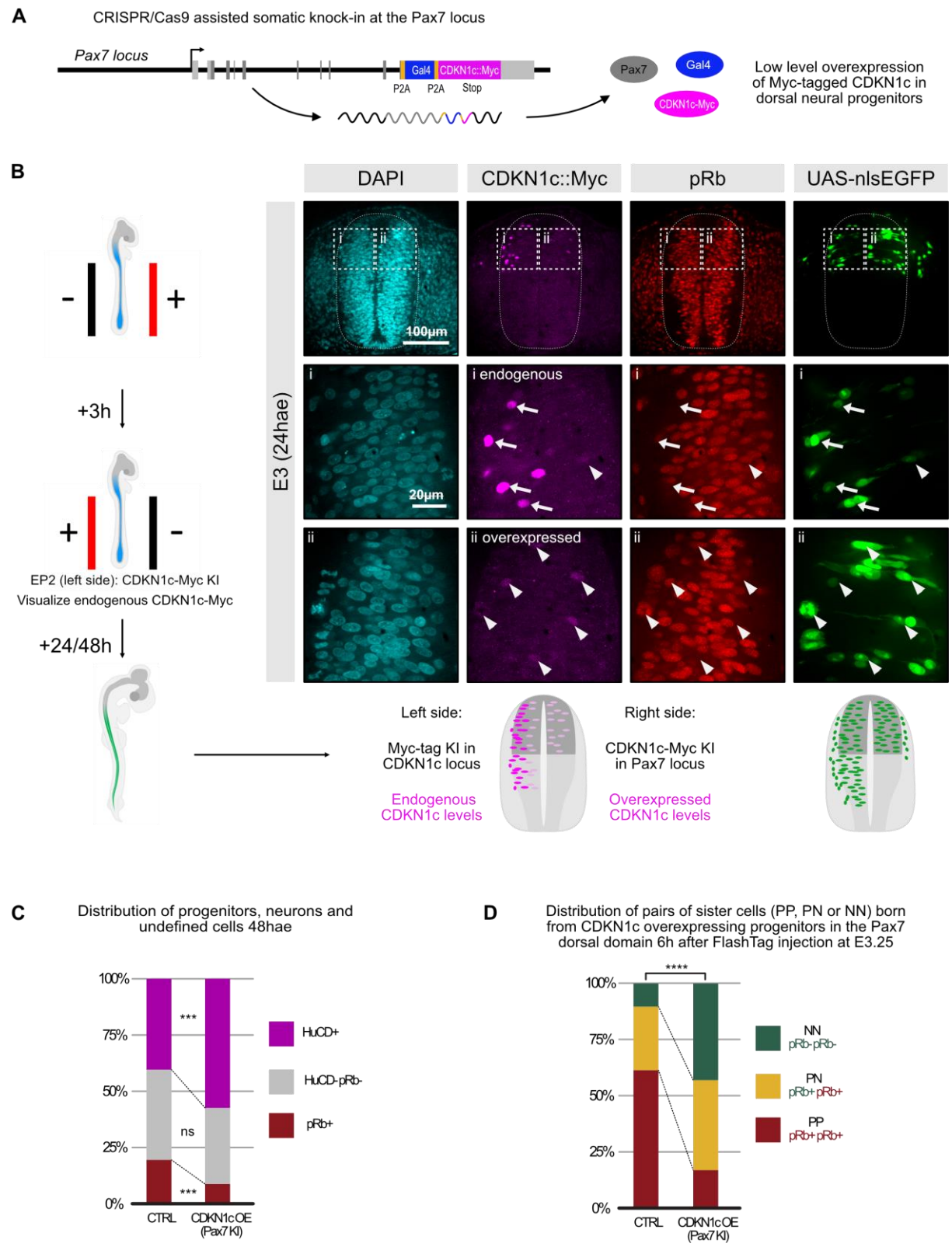

Figure 4 : Premature expression of CDKN1c at low levels in proliferative progenitors converts them to a neurogenic mode of division

A Schematic representation of the modified Pax7 locus driving low-level expression of CDKN1c-Myc and Gal4-VP16 in dorsal progenitors. Pax7 (gray), Gal4-VP16 (blue) and CDKN1c-Myc (magenta) coding sequences are transcribed from the Pax7 locus and co-translated. The insertion of P2A pseudo-cleavage sites (orange) between the three sequences ensures that all three proteins are present as three independent proteins, each performing its own function in the cell (see Supp Figure 4 and Methods for further details)

B Pax7-driven exogenous expression of CDKN1c in dorsal progenitors mimics the levels of CDKN1c expression in neurogenic progenitors. A bilateral electroporation scheme was used to compare Pax7-driven levels of CDKN1c expression (electroporation 1, right side hemi-tube, knock-in of CDKN1c-Myc in the Pax7 locus) with endogenous CDKN1c levels (electroporation 2, left side hemi-tube, knock-in of a Myc tag in the CDKN1c locus). The level of CDKN1c-Myc (magenta) expression driven by Pax7 is low and restricted to the ventricular region, where it is comparable to the endogenous levels of CDKN1c-Myc expression in the contralateral side (i and ii, arrowheads). Pax7 driven CDKN1c never reaches the high levels of endogenous CDKN1c observed in the intermediate zone (i, arrows), indicating that exogenous expression is restricted to progenitors and fades off in prospective neurons.

C Distribution of the pRb positive progenitors (red), HuCD positive neurons (green) and undefined cells (double pRB/ HuCD negative, gray) in Pax7-CDKN1c overexpression or control conditions 48 hours after electroporation (hae). ns, $p > 0.05$; *** $p < 0.005$, unpaired Student's t test.

D Diagram indicating the percentage of P-P, P-N, and N-N clones for control and Pax7-CDKN1c overexpression conditions. CDKN1c-Myc and Gal4 were inserted in the Pax7 locus, and KI events in dorsal progenitors were revealed thanks to a UAS-nls-EGFP reporter. For the control condition, we used a KI construct where Gal4 alone is inserted downstream of Pax7. P-P, P-N, and N-N stand for divisions producing two progenitors, one progenitor and one neuron, or two neurons, respectively. The distribution of P-P, P-N and N-N clones between both conditions was compared using a Chi-2 test , ****$p < 0.05$.

Mida et al., Figure 5

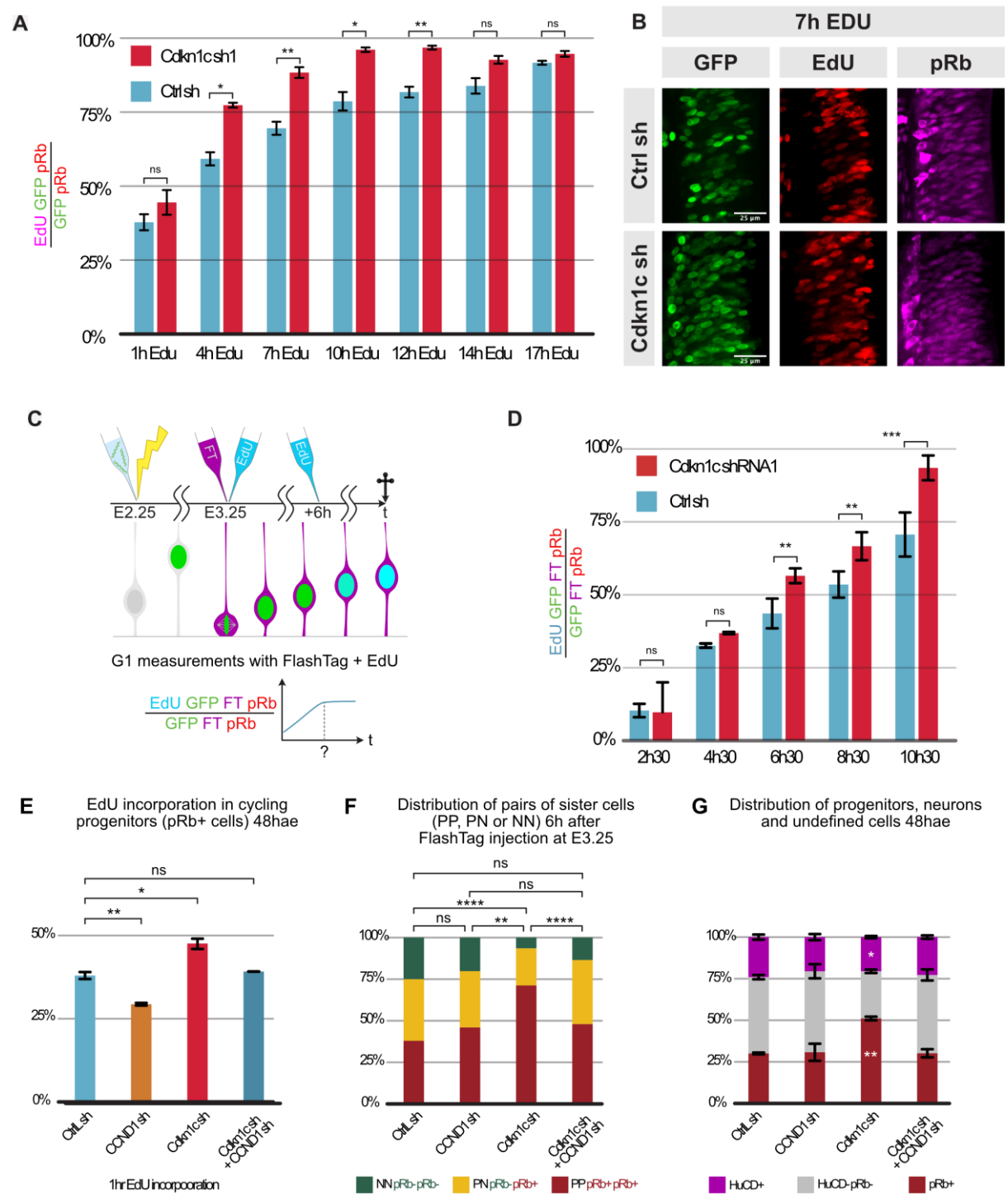

Figure 5 : CDKN1c controls G1 phase duration in neural progenitors, and its effects on cell cycle duration and neurogenesis counteract CCND1 activity.

A. Distribution of the electroporated progenitors in S phase in the electroporated progenitor population in shRNA 1 and control conditions. The columns represent the percentages of (Edu/pRB/GFP triple positive cells) in the electroporated progenitor (GFP/pRb double positive cells) population of control (blue) and shCDKN1c (red) conditions at each time point. For time points beyond 6 hours, a second EdU injection was performed 6 hours after the first one. EdU, 5-ethynyl-20-deoxyuridine; ns : $p > 0.05$; *, $p < 0.05$; **, $p < 0.01$ (Student's unpaired t test).

B. EdU incorporation (red) in representative transverse sections of the chick neural tube (thoracic level) 7h after EdU administration started at E3 (HH st22), stained with pRb antibody (magenta) to label progenitors, and GFP antibody to identify electroporated cells. Scale bar, 25 µm.

C. Schematic representation of the experimental strategy to measure G1 length. Embryos were electroporated with shRNA1 or control plasmids at E2.25 (HH13-14; top left, yellow thunder). One day later, FlashTag injection in the neural tube and EdU administration in ovo were performed simultaneously. Embryos were harvested at consecutive time point every 2 hours between 2:30 and 10:30. For time points beyond 6 hours, a second EdU injection was performed 6 hours after the first one. EdU, 5-ethynyl-20-deoxyuridine;

D. Dynamics of EdU incorporation in a FlashTag-positive cohort of electroporated progenitors. The columns represent the percentages of Edu-positivity in FlashTag/pRb/GFP triple positive cells in shRNA (red) and control (blue) populations at each time point. ns, $p > 0.05$; **,$p < 0.01$; ***, $p < 0.001$ (Student's unpaired t test).

E. Diagram indicating the proportion of EdU positive progenitors after a 1hr pulse of EdU at E4. The columns represent the percentages of EdU-positive cells in electroporated progenitors (pRb/GFP double positive) in control, single CCND1, single Cdkn1c and double CCND1/Cdkn1c shRNA conditions. ns, $p > 0.05$; *, $p < 0.05$; **, $p < 0.01$ (Student's unpaired t test).

F. Diagram indicating the percentage of P-P, P-N, and N-N pairs of sister cells in control, single CCND1, single Cdkn1c and double CCND1/Cdkn1c shRNA conditions. P-P, P-N, and N-N stand for divisions producing two progenitors, one progenitor and one neuron, or two neurons, respectively. The distribution of P-P, P-N and N-N clones between control and shRNA was compared using the Chi-2 test, **$p < 0.05$; ****, $p<0.005$.

G. Distribution of the progenitor (pRb positive cells), neurons (HuCD positive cells) and undefined cells (double pRb/HuCD negative) at E4 in control, single CCND1, single Cdkn1c and double CCND1/Cdkn1c shRNA conditions. ns, $p > 0.05$; *, $p < 0.05$; **, $p < 0.01$ (unpaired Student's t test relative to control sh).

Hae: hours after electroporation

Mida et al., Supplementary Figure 1

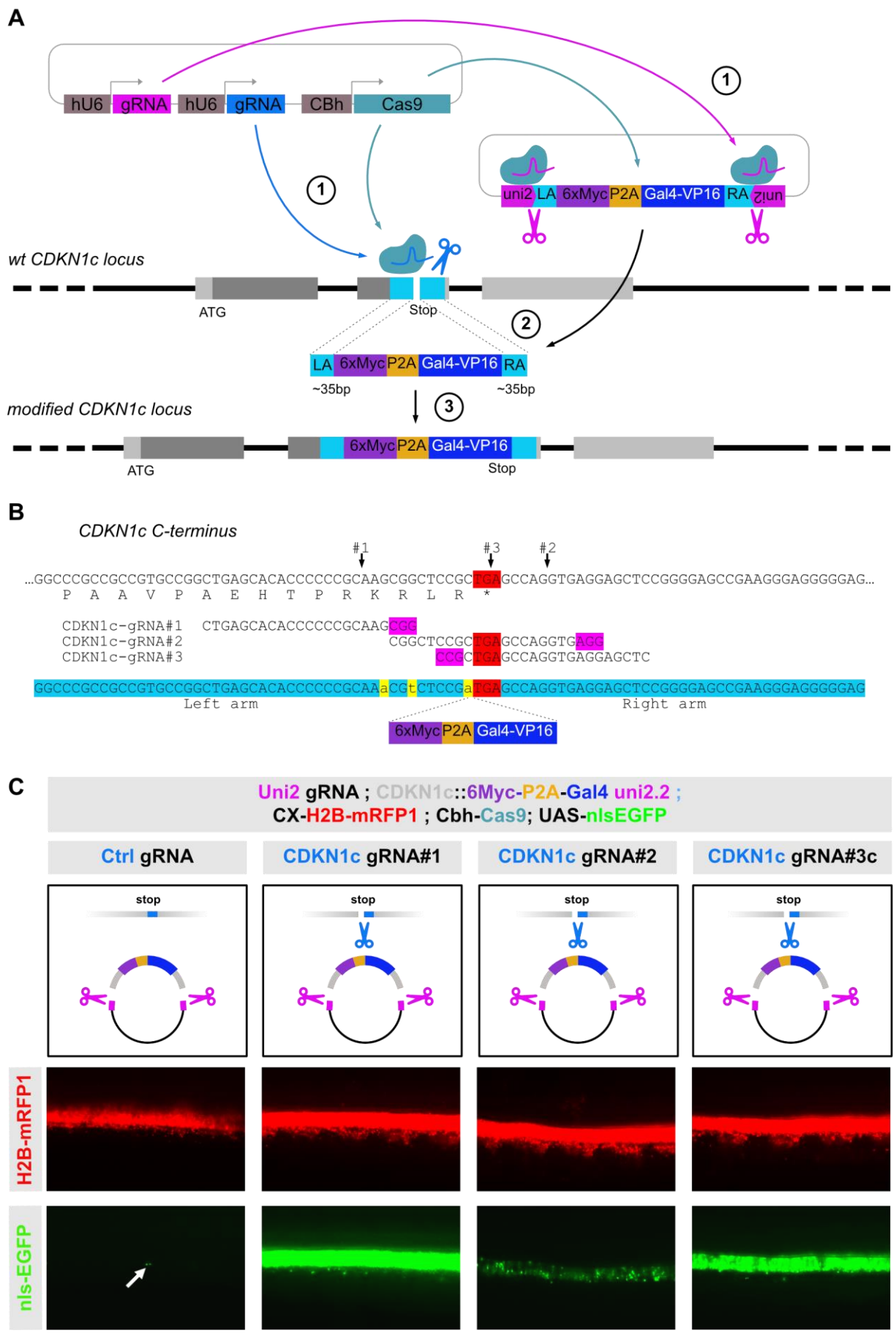

Supplementary Figure 1: somatic knock-in strategy to tag the endogenous CDKN1c protein and monitor the dynamic expression of the locus in spinal cord progenitors

A. "micro-homology mediated end joining" (MMEJ) strategy used for the somatic KI. Somatic KI is achieved by the combined electroporation of two plasmids. The donor plasmid carries the short arms of homology (<35bp) to the CDKN1c locus at the level of the C-terminus, flanking 6 Myc tags in frame with CDKN1c coding sequence, a P2A pseudo cleavage sequence and the Gal4-VP16 synthetic transcription factor. This donor cassette is flanked on both sides by target sites for a "universal" guide RNA (uni2 gRNA) designed to trigger linearization of vector and release of the donor cassette as a linear double-stranded DNA fragment in the electroporated cells. The CRISPR vector produces the Cas9 protein, and two gRNA expression cassettes, respectively expressing the uni2 gRNA targeting the donor vector for linearization, and the locus specific gRNA the genomic sequence.

B. Details of the targeted genomic sequence for endogenous tagging of the CDKN1c locus. Genomic sequence at the level of CDKN1c C-terminus (top), sequence of the three gRNAs tested in this study (middle), and sequence of the arms of homology used in the MMEJ construct (bottom, sequence highlighted in blue). The 3 bases highlighted in yellow represent silent base changes introduced in the left arm of homology to prevent recognition and cleavage of the donor vector by gRNA#1. Arrows indicate the theoretical cut sites of the three gRNAS on the target locus.

C. Validation of the efficiency and specificity of the KI strategy: the donor vector was coelecrtoporated with CRISPR vectors expressing either a Control gRNA (Ctrl gRNA) or one of the three gRNAS targeting the CDKN1c locus. A UAS-nls-EGFP vector was included in the electroporation mix to report expression of the Gal4-VP16 transcription factor that is targeted to the locus. Finally, an electroporation reporter (CX-H2B-mRFP) was added to monitor the quality of electroporation. One representative embryo is shown for each condition, with similar electroporation level (red). gRNA1 led to a strong GFP signal (green), showing the greatest efficiency. gRNA3 was slightly less efficient, and gRNA2 yielded a much lower signal. Specificity is demonstrated by the virtual absence of background GFP signal when the control gRNA is used (white arrow points to a single GFP+ cell observed in the control embryo).

Mida et al., Supplementary Figure 2

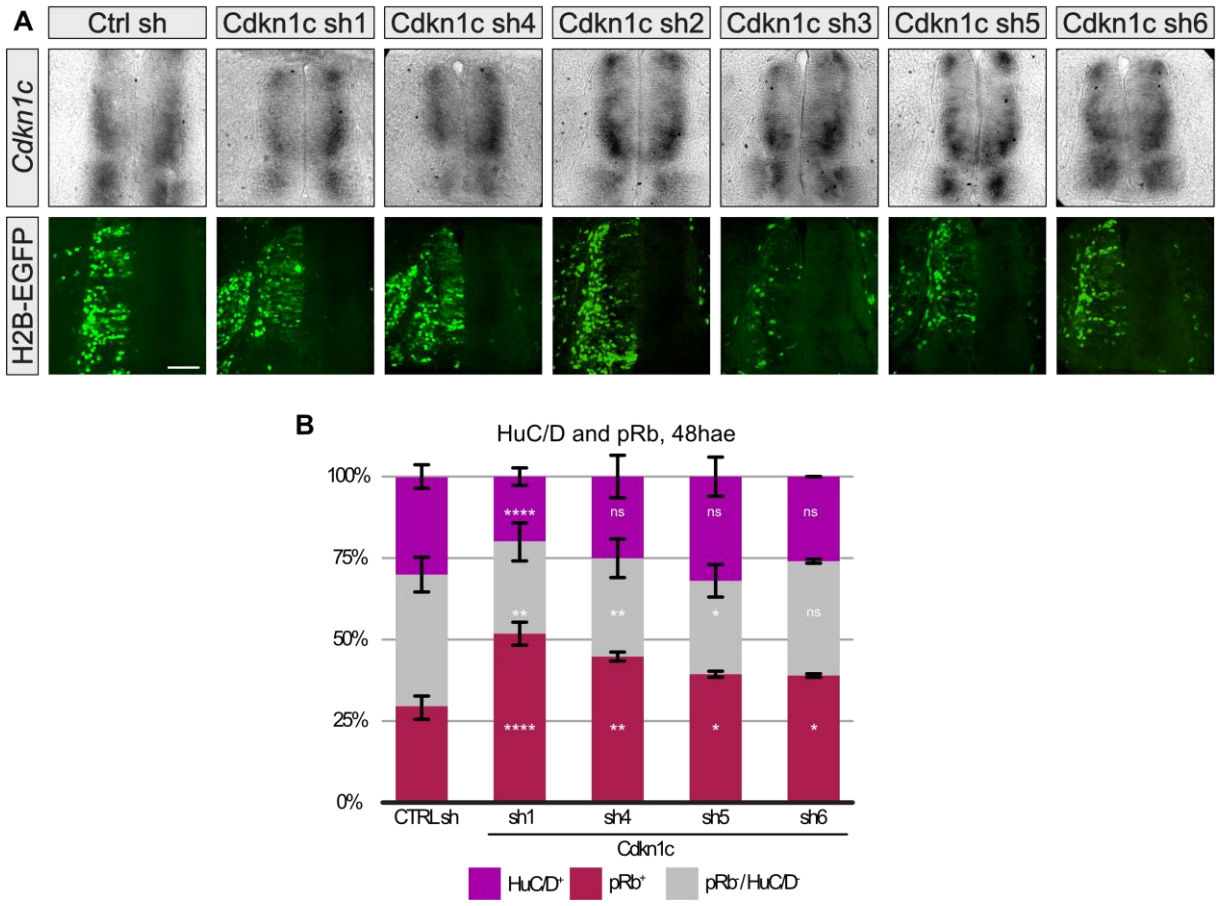

Supplementary Figure 2: partial knock down of CDKN1c expression in spinal cord progenitors and prospective neurons via shRNA delays neurogenesis

A mRNA expression of Cdkn1c in chick embryonic neural tube after electroporation of each of the six shRNA. In situ hybridization on cryosections of thoracic region of chick embryo coupled to GFP immunofluorescence. Upper panel: visible downregulation of CDKN1C mRNA was only observed with shRNA 1 and to a lesser extent shRNA 4 conditions, while comparable mRNA expression to the control condition was observed with the other shRNAs (compare left versus right hemitube). Lower panel: Corresponding level of electroporation for each embryo (GFP immunofluorescence). Scale bar: 50µm

B Distribution of the pRb positive progenitors (red), HuCD positive neurons (green) and undefined cells (double pRB/ HuCD negative, gray) in shRNA 1, 4, 5, 6 or control conditions at E4 48 hours after electroporation (hae). (Ctrl and sh1 are identical to Figure 2B) ns, $p > 0.05$; *, $p < 0.05$; **, $p < 0.01$; ****, $p < 0.001$ (unpaired Student's t test relative to control sh population).

Hae: hours after electroporation

Mida et al., Supplementary Figure 3

Time course of pRb saturation in a cohort of FlashTag labelled cells at E2 and E3

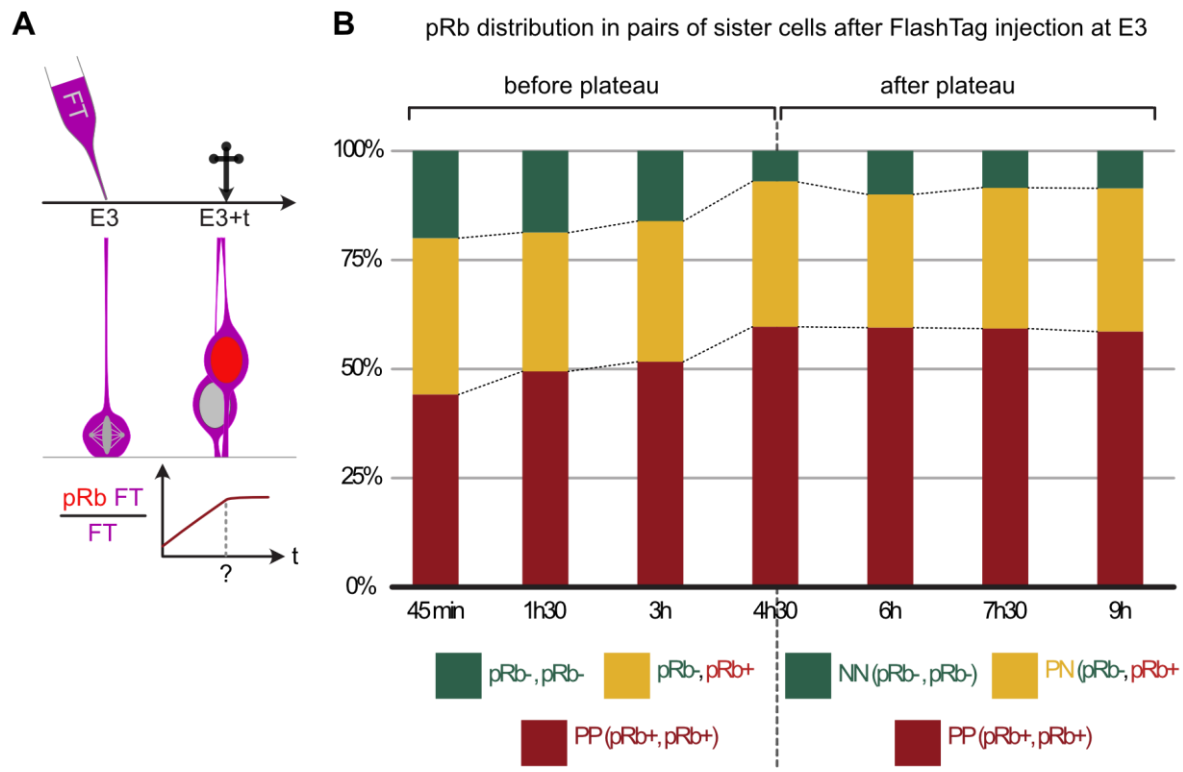

C

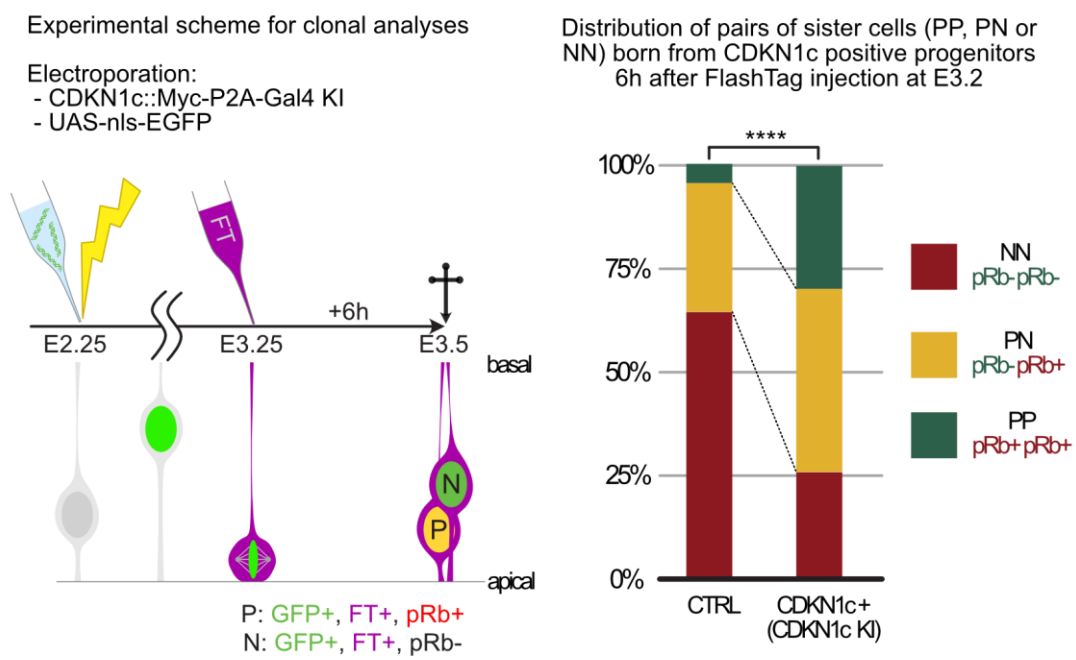

Supplementary Figure 3: pRb is a reliable marker of progenitor cells 6 hours after mitosis

A Schematic representation of analysis of pRb expression in pairs of sisters. Embryos are injected with FlashTag at to label a synchronous cohort of mitotic progenitors. They are collected at different timepoints after injection to determine at which time point pRb positivity in sister pairs will reach a plateau, corresponding to the time when all progenitors can be unambiguously identified using pRb as a marker.

B Time course of pRb expression in pairs of sister cells at consecutive time points after FlashTag injection. FlashTag injection was performed at HH17-18 (E3), embryos were harvested at the indicated timepoints after injection, and thoracic vibratome sections were immunostained with pRb antibody to evaluate the pRb status in pairs of FlashTag positive sister cells. The proportion of pairs with two pRb positive cells (green), one pRb-positive cell (yellow) or zero pRb positive cell (red) is stable after 4h30, indicating that after that time point, pRb status becomes a reliable indicator for fate analyses in FlashTag-labelled pairs of sister cells.

C CDKN1c-positive progenitors are more neurogenic. The proportion of PP, PN and NN pairs born from CDKN1c-positive progenitors was compared to the overall progenitor population. A knock-in of the Gal4 reporter in the CDKN1c locus was performed at E2.25 (top left, yellow thunder) and FlashTag was injected 24hours later. Sister cells born from CDKN1c-positive progenitors dividing at the time of FlashTag injection were identified on the basis of the expression of a UAS-nls-EGFP reporter and FlashTag positivity. The proportion of PP, PN, and NN pairs in the general population was analyzed in FlashTag-positive cells in the contralateral side of the same transverse sections. The CDKN1c-positive population of progenitors is significantly more neurogenic than the whole population at that stage. Chi-2 test, ****, $p<0.005$.

Mida et al, Supplementary Figure 4

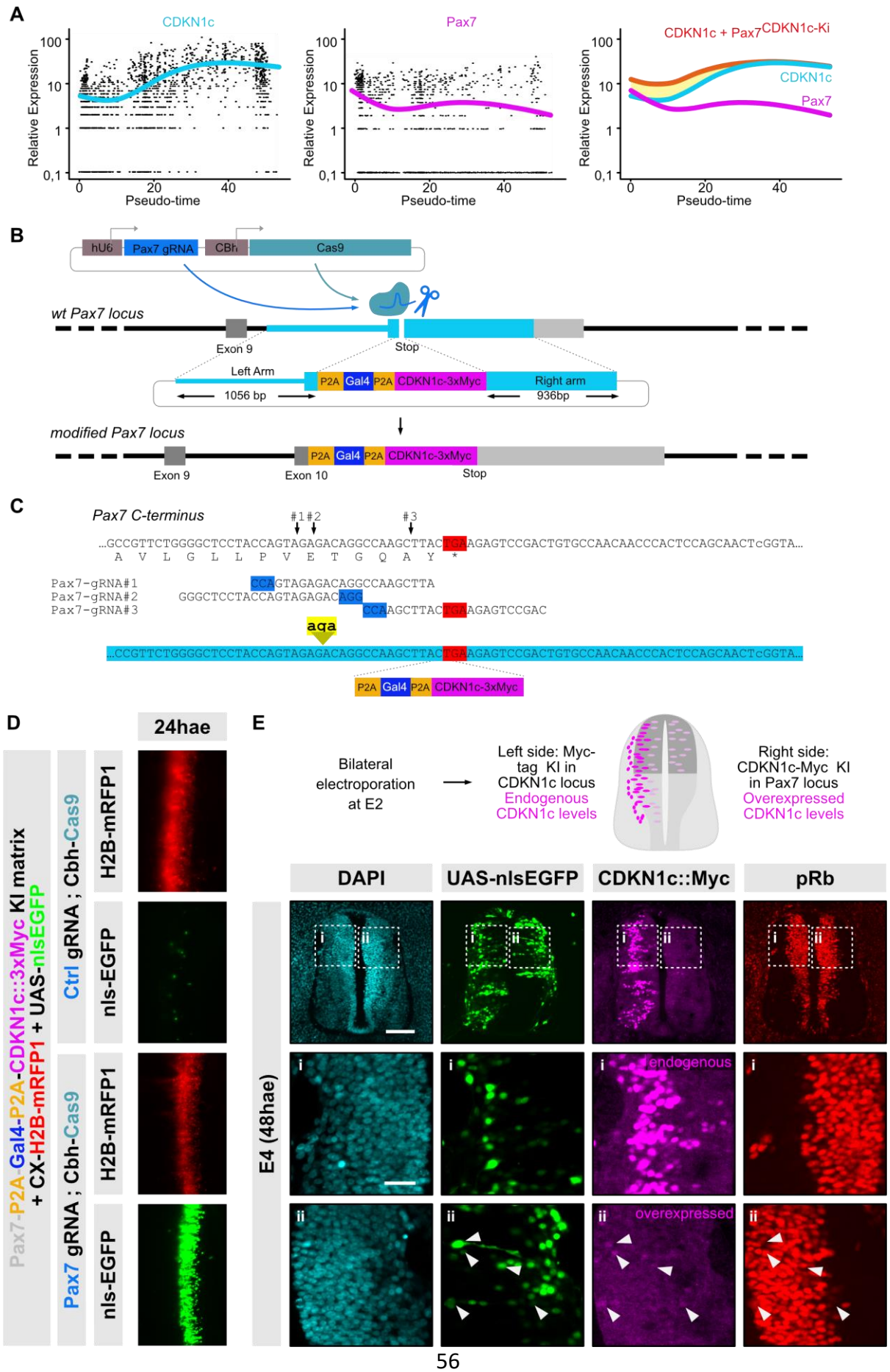

Supplementary Figure 4 : principle and validation of CDKN1c knock-in at the Pax7 locus for moderate overexpression of CDKN1c in dorsal neural progenitors before the neurogenic transition.

A Expression levels of CDKN1c and Pax7 transcripts along the pseudo-time axis from the chick scRNASeq analysis. CDKN1c expression has very low levels in "early" progenitors (left part of the pseudotime axis) and increases in more mature progenitors, before peaking in differentiating neurons. Pax 7 expression levels in "early" progenitors are slightly higher than those of CDKN1c, and later go down in postmitotic cells. The right panel shows an estimated cumulative expression (red) line) of endogenous (blue) and Pax7-driven (magenta) CDKN1c levels upon knock-in of CDKN1c coding sequences in the Pax7 locus, which should result in premature expression in early progenitors, but no overexpression in newborn neurons.

B "homology directed repair" (HDR) strategy used to drive low-level expression of CDKN1c-Myc and Gal4-VP16 in dorsal progenitors from the Pax7 locus. Somatic KI is achieved by the combined electroporation of two plasmids. The donor plasmid carries long arms of homology (~1Kbp) to the Pax7 locus at the level of the C-terminus in exon 10. The arms of homology flank an "in-frame" knock-in cassette consisting in a P2A pseudo-cleavage site, the Gal4-VP16 synthetic transcription factor, a second P2A pseudo-cleavage site and the CDKN1c coding sequence fused to 3 C-terminal Myc tags. The other vector expresses the Cas9 protein and a gRNA that targets the genomic region of Pax7 upstream of the stop codon. Upon successful knock-in insertion, Pax7 (gray), Gal4-VP16 (blue) and CDKN1c-Myc (magenta) coding sequences will be transcribed from the Pax7 locus and co-translated. The insertion of P2A pseudo-cleavage sites (orange) between the three sequences will ensure that all three proteins are present as three independent proteins, each performing its own function in the cell**.**

C. Details of the targeted genomic sequence at the C-terminus of the Pax7 locus. Genomic sequence at the level of Pax7 C-terminus (top), sequence of the three independent gRNAs targeting this region (middle), and sequence of the arms of homology surrounding the knock-in cassette (bottom, sequence highlighted in blue). To avoid possible targeting of the donor arms by gRNAs #1 and #2, 3 bases (highlighted in yellow) were inserted 5 amino acids upstream of the Pax7 stop codon, effectively destroying recognition. Note that this introduces an Arginine residue (AGA) in the Pax7 sequence.

D. Validation of the efficiency and specificity of the KI strategy: Imaging of the neural tube directly *in ovo*. The donor vector was coelectroporated in the chick neural tube together with a dual vector expressing the Cas9 nuclease and either a Control gRNA (Ctrl gRNA) or the gRNA targeting the Pax7 locus. A UAS-nls-EGFP vector was included in the electroporation mix to report expression of the Gal4-VP16 transcription factor that is targeted to the locus. Finally, an electroporation reporter (CX-H2B-mRFP) was added to monitor the quality of electroporation. One representative embryo is shown for each condition, with similar electroporation level (red). Specificity is demonstrated by the virtual absence of background GFP signal when the control gRNA is used (compared to the massive GFP signal obtained with Pax7 gRNA, only 4 GFP+ cells are observed in the control embryo). In addition, specificity was demonstrated by the dorsally restricted expression of the GFP signal in the Pax7 domain on transverse section (see for example, GFP signal in the right hemitube in panel E).

E Pax7-driven exogenous expression of CDKN1c in dorsal progenitors mimics the levels of CDKN1c expression in neurogenic progenitors at E4. A bilateral electroporation scheme was used to compare Pax7-driven levels of CDKN1c expression (electroporation 1, right side hemitube, knock-in of CDKN1c-Myc in the Pax7 locus) with endogenous CDKN1c levels

(electroporation 2, left side hemi-tube, knock-in of a Myc tag in the CDKN1c locus). The level of CDKN1c-Myc (magenta) expression driven by Pax7 is low and restricted to the ventricular region, where it is comparable to the endogenous levels of CDKN1c-Myc expression in the contralateral side (i and ii, arrowheads). Pax7 driven CDKN1c never reaches the high levels of endogenous CDKN1c observed in the intermediate zone (i, arrows), indicating that exogenous expression is restricted to progenitors and fades off in prospective neurons. Note that although very few cells with a detectable CDKN1c-Myc expression are observed in the overexpressed condition, the UAS-nls-EGFP reporter is widely expressed, indicating strong electroporation and knock-in efficiency. The weak Myc signal is explained by a different stability and posttranslational regulation between CDKN1c-Myc and Gal4-VP16, and amplification of the nls-EGFP via the Gal4/UAS system, leading to perdurance of the GFP signal after Pax7 driven expression of CDKN1c has disappeared. Scale bars, 100µm in top row and 30 µm in close ups.

Mida et al., Supplementary Figure 5

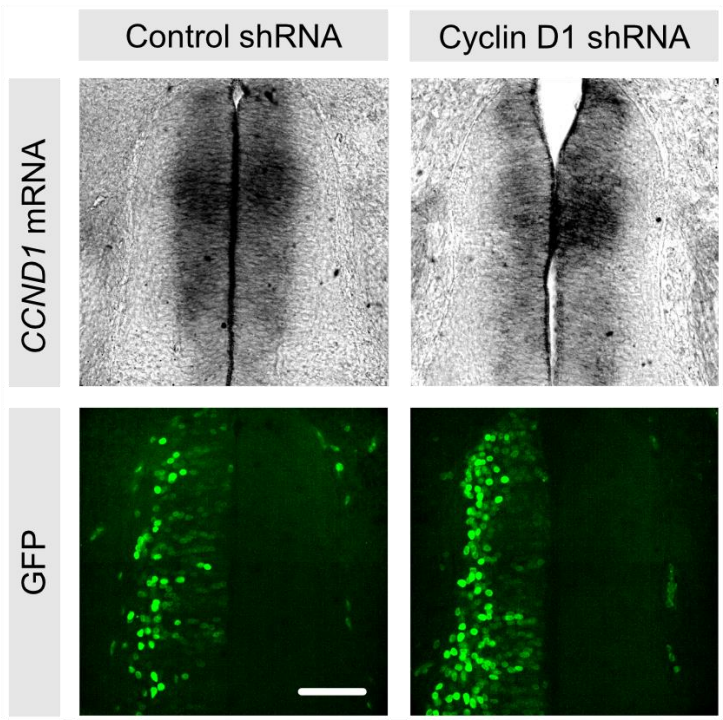

Supplementary Figure 5 : Decreased *CCDN1C* mRNA expression in chick embryonic neural tube one day after shCCND1 electroporation.

In situ hybridization of *CCND1* probe on transverse cryo-sections of chick embryonic neural tube followed by anti-GFP immunostaining to reveal electroporated cells. Scale bars: 100µm